CMS Physics Analysis Summary

Contact: cms-pag-conveners-higgs@cern.ch 2012/11/16

Combination of standard model Higgs boson searches and measurements of the properties of the new boson with a mass near 125 GeV

The CMS Collaboration

Abstract

Results are presented from searches for the standard model (SM) Higgs boson in proton-proton collisions at $\sqrt{s}$ = 7 and 8 TeV, using data samples corresponding to integrated luminosities of up to 5.1 fb^{-1} at 7 TeV and up to 12.2 fb^{-1} at 8 TeV. The search is performed in the mass range 110–1000 GeV in five decay modes: $\gamma\gamma$, ZZ, WW, $\tau\tau$, and bb. Updated results are presented except for the $\gamma\gamma$ mode. The significance of the recently discovered boson is now $6.9\,\sigma$. Its mass is measured to be 125.8 $\pm$ 0.4 (stat) $\pm$ 0.4 (syst) GeV. The event yields obtained by the different analyses targeting specific decay modes and production mechanisms are consistent with those expected for the SM Higgs boson. The best-fit signal strength for all channels combined, expressed in units of the SM Higgs boson cross section, is 0.88$\pm$0.21 at the measured mass. The consistency of the couplings of the observed boson with those predicted for the SM Higgs boson is tested in various ways, and no significant deviations are found. Under the assumption that the observed boson has spin zero, the data disfavour the pseudo-scalar hypothesis 0^- with a CL_s value of 2.4%.

1 Introduction

Understanding the mechanism for electroweak symmetry breaking is one of the primary goals of the physics programme at the Large Hadron Collider (LHC). In the standard model [1–3], this symmetry breaking is achieved by introducing a complex scalar doublet, leading to the prediction of the Higgs boson (H) [4–9].

In this note we report on the combination of searches for the SM Higgs boson carried out in proton-proton collisions at $\sqrt{s} = 7$ (2011 data) and 8 TeV (2012 data) using the Compact Muon Solenoid (CMS) detector [10] at the LHC: the analysed data correspond to integrated luminosities of up to 5.1 fb^{-1} and 12.2 fb^{-1}, respectively. The search range is extended up to 1000 GeV. We also present measurements of the properties of the recently observed boson with a mass near 125 GeV by CMS [11] and ATLAS [12].

The CMS detector [13] consists of a barrel assembly and two endcaps, comprising, in successive layers outwards from the collision region, the silicon pixel and strip tracker, the lead tungstate crystal electromagnetic calorimeter, the brass/scintillator hadron calorimeter, the superconducting solenoid, and gas-ionization chambers embedded in the steel return yoke for the detection of muons.

Early phenomenological work on Higgs boson production and decay can be found in Refs. [14–20]. There are four main production modes for Higgs boson production in pp collisions at $\sqrt{s} = 7 - 8$ TeV. The gluon-gluon fusion production mode has the largest cross section, followed in turn by vector boson fusion (VBF), associated WH and ZH production, and production in association with top quarks, $\mathrm{t\bar{t}H}$. The cross sections for the Higgs boson production modes and the decay branching fractions, together with their uncertainties, are taken from Refs. [21–23] and are derived from Refs. [24–68]. The total cross section at $\sqrt{s}$ =7 (8) TeV varies from 23 (29) to 0.03 (0.06) pb in the explored Higgs boson mass range of 110–1000 GeV.

The relevant decay modes of the SM Higgs boson depend strongly on its mass m_{H}. The results presented here are based on the following five decay modes: $\mathrm{H} \to \gamma\gamma$, $\mathrm{H} \to \tau\tau$, followed by leptonic and hadronic decays of the τ-leptons, $\mathrm{H} \to \mathrm{bb}$, $\mathrm{H} \to \mathrm{WW}$, followed by $\mathrm{WW} \to \ell\nu\ell\nu$ and $\ell\nu\mathrm{qq}$ decays, and $\mathrm{H} \to \mathrm{ZZ}$, followed by ZZ decays to 4ℓ, $2\ell 2\nu$, $2\ell 2\mathrm{q}$, and $2\ell 2\tau$. Here and throughout, ℓ stands for electrons or muons and q for quarks. For simplicity, $\mathrm{H} \to \tau^+\tau^-$ is denoted as $\mathrm{H} \to \tau\tau$, $\mathrm{H} \to \mathrm{b\bar{b}}$ as $\mathrm{H} \to \mathrm{bb}$, etc. The WW and ZZ decay modes are used over the entire explored mass range. The $\gamma\gamma$, $\tau\tau$, and bb decay modes are used only for $m_{\mathrm{H}} < 145$ GeV since their expected sensitivities are not significant compared to WW and ZZ for higher Higgs boson masses.

For a given Higgs boson mass hypothesis, the search sensitivity depends on the production cross section of the Higgs boson, its decay branching fraction into the chosen final state, the signal selection efficiency, the mass resolution, and the level of standard model backgrounds in the same or a similar final state. For low values of the Higgs boson mass, the $\mathrm{H} \to \gamma\gamma$ and $\mathrm{H} \to \mathrm{ZZ} \to 4\ell$ channels play a special role due to the excellent mass resolution for the reconstructed diphoton and four-lepton final states, respectively. The $\mathrm{H} \to \mathrm{WW} \to \ell\nu\ell\nu$ channel provides high sensitivity but has relatively poor mass resolution due to the presence of neutrinos in the final state. The sensitivity in the bb and $\tau\tau$ decay modes is reduced due to the large backgrounds and poor mass resolutions. In the high mass range, the sensitivity is driven by the WW and ZZ modes.

2 Search channels

The results obtained by combining information from many search channels are presented in this note. A summary of all analyses used in the combination is presented in Table 1 where we list their main characteristics, namely: the exclusive final states, the mass range of the search, the integrated luminosity used, and the approximate instrumental mass resolution. The presence of a signal or an upward fluctuation of the background in one of the channels, at a certain value of the Higgs boson mass, is expected to manifest itself as an excess extending around that value for a range corresponding to the m_{H} resolution.

Table 2 shows modes used in the searches for a light Higgs boson ($110 < m_{\mathrm{H}} < 145\,\mathrm{GeV}$). The search modes are grouped in this table by the production and decay modes specifically targeted by the corresponding analyses. The naming convention reflects the signature targeted. None of these signatures is 100% pure.

As an illustration of the search sensitivity of the different channels, Fig. 1 shows the median expected 95% CL upper limit on the ratio of the signal cross section, σ, and the predicted SM Higgs boson cross section, σ_{SM}, as a function of the SM Higgs boson mass hypothesis. A channel showing values below unity (dotted line) would be expected to be able to exclude a Higgs boson of that mass at 95% CL. Fig. 2 shows the expected sensitivities for the observation of the SM Higgs boson in terms of p-values and significances. The methods used for deriving limits and p-values are described in Section 3. A caution regarding low p-values is in Sec. 3.2.

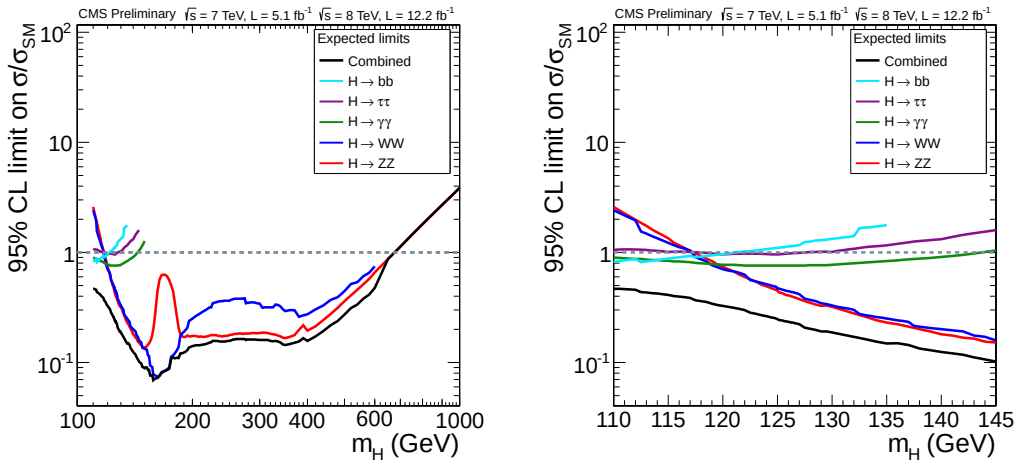

Figure 1: The median expected 95% CL upper limits on the cross section ratio $\sigma/\sigma_{\mathrm{SM}}$ in the absence of a Higgs boson as a function of the SM Higgs boson mass in the range 110–1000 GeV (left) and 110–145 GeV (right), for the five Higgs boson decay channels. Here σ_{SM} denotes the cross section predicted for the SM Higgs boson. A channel showing values below unity (dotted line) would be expected to be able to exclude a Higgs boson of that mass at 95% CL. The jagged structure in the limits for some channels results from the different event selection criteria employed in those channels for different Higgs boson mass sub-ranges.

The high mass region

The VV final states are sensitive up to very high masses (i.e. 1000 GeV). This mass region has been analysed assuming the SM hypothesis. The m_{VV} lineshape has been corrected to match the results presented in Ref. [41, 81, 82] where the Complex-Mass Scheme (CPS) for the Higgs propagator is utilised. Moreover, in the gluon-gluon fusion production channel the effects on the lineshape due to interference between the Higgs-boson signal and the $gg \to VV$ background have been included, as suggested in Ref. [83].

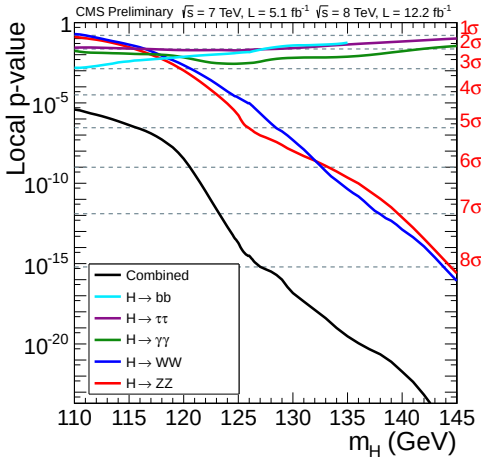

Figure 2: The expected sensitivities for the observation of the SM Higgs boson in terms of p-values and significances is shown as a function of the SM Higgs boson mass in the range 110–145 GeV (left), for the five Higgs boson decay channels. The jagged structure in the limits for some channels results from the different event selection criteria employed in those channels for different Higgs boson mass sub-ranges.

The theoretical uncertainty (THU) on the shape of the resonance due to missing higher orders (NLO) in the interference between background and signal is included, as well as the uncertainties due to electroweak corrections, as suggested in Refs. [81, 83]. The contribution of the interference away from the peak of the resonance has sizable effects on the normalization only for those final states where the VV invariant mass cannot be fully reconstructed. This correction has been included, with the corresponding THU, in the $lvjj$ final state, as suggested in Ref. [83].

For the $VV \to lvlv$ final state, phenomenological studies are available [84–86] and, in the present analysis, corrections to the normalization to include interference effects at Leading Order have been applied with 100% uncertainty. The effect of interference on Vector Boson fusion production is still under study.

2.1 $H \to \gamma\gamma$

For this combination, the $H \to \gamma\gamma$ analysis is as published in Ref. [11] and has not been updated with additional data. The analysis, discussed in detail in Ref. [69], is focused on the search for a narrow peak in the diphoton mass distribution. The event sample is split into two mutually exclusive classes: (i) diphoton events with one forward and one backward jet, consistent with the VBF topology, and (ii) all remaining events. This division is motivated by the consideration that there is a better signal-to-background ratio in the first class than in the second. For the 8 TeV data, the dijet class is split into two sub-classes: events with low and high dijet mass m_{jj}. The non-dijet class, containing over 99% of the data, is subdivided into four sub-classes based on the output of a multivariate discriminant that assigns a high score to signal-like events, based on (i) an event-by-event estimate of the diphoton mass resolution, (ii) a photon identification score for each photon, and (iii) kinematic information about the photons and the diphoton system. The photon identification score is obtained from a multivariate analysis (MVA) discriminant that uses shower shape information and isolation variables to separate prompt photons from those arising from jets. The background in the signal region is estimated from a fit to the observed diphoton mass distribution in data.

2.2 $H \to bb$

The $H \to bb$ search [70] concentrates on Higgs boson production in association with a W or Z boson, in which the focus is on the following decay modes: $W \to e\nu/\mu\nu$ and $Z \to ee/\mu\mu/\nu\nu$. The $Z \to \nu\nu$ decay is identified by requiring large missing transverse energy E_T^{miss}, defined as the modulus of the vector $\vec{E}_T^{miss}$ computed as the negative of the vector sum of the transverse momenta of all reconstructed objects in the detector (leptons, photons, and charged/neutral hadrons) which are not found to arise from additional interactions. The Higgs boson candidate is reconstructed by requiring two b-tagged jets. The search is divided into events where the vector bosons have medium or large transverse momentum and recoil away from the candidate Higgs boson. A multivariate regression algorithm to better estimate the b-jet p_T is trained on jets in simulated signal events and achieves a final dijet mass resolution of 8-9% for m_H = 125 GeV. The performance of the regression algorithm is checked in data using W, Z+jets and $t\bar{t}$ events. Events with higher transverse momentum bosons have smaller backgrounds and a better dijet mass resolution. In the 8 TeV analysis, for all final states except $Z \to \ell\ell$, the large transverse momentum events are further divided depending on whether they satisfy tight or loose b-tagging requirements. A multivariate analysis technique, trained on simulated signal and background events for several different values of the Higgs boson mass, is used to separate signal and background events. The rates of the main backgrounds, consisting of W/Z + jets and top-quark events, are derived from signal-depleted control samples in data. The WZ and ZZ backgrounds with a Z boson decaying to a pair of b-quarks, as well as the single-top background, are estimated from simulation. The MVA output distribution is used as the final discriminant in the limit setting.

The search for $H \to bb$ is also performed using events where the Higgs boson is produced in association with a top-quark pair [71]. This analysis uses events where the top-quark pair decays to either the lepton-plus-jets ($t\bar{t} \to \ell\nu jjbb$) or dilepton ($t\bar{t} \to \ell\nu\ell\nu bb$) final state. The major background in this search is top-pair production accompanied by extra jets. We use a MVA to discriminate between background and signal events. The rates of background processes are estimated from theoretical expectations, and are further constrained in-situ through the inclusion of background enriched samples in the extraction of the final limit.

2.3 $H \to \tau\tau$

The $H \to \tau\tau$ search [72] is performed using the final-state signatures $e\mu$, $\mu\mu$, $e\tau_h$, $\mu\tau_h$, $\tau_h\tau_h$, where electrons and muons arise from leptonic τ-decays and τ_h denotes τ decaying hadronically. Each of these categories is further divided into two exclusive sub-categories based on the number and the type of the jets in the event: (i) events with one forward and one backward jet, consistent with the VBF topology, (ii) events with at least one high p_T hadronic jet but not selected in the previous category. The second category is further split in two bins of reconstructed τ p_T. In each of these categories, we search for a broad excess in the reconstructed $\tau\tau$ mass distribution. The zero-jet category is used to constrain background normalizations, identification efficiencies, and energy scales. The main irreducible background, $Z \to \tau\tau$ production, and the largest reducible backgrounds (W + jets, multijet production, $Z \to ee$) are evaluated from various control samples in data. The treatment of the VBF category has been changed with respect to Ref. [11].

The search for $H \to \tau\tau$ decays produced in association with a W or Z boson is conducted in events with three or four leptons in the final state [73]. The WH analysis selects events which have same charged electrons or muons and a hadronically-decaying tau: $e^+e^+\tau_h^-$ and $\mu^+\mu^+\tau_h^-$. The ZH analysis is performed in events with an identified $Z \to ee$ or $Z \to \mu\mu$ decay

and a Higgs boson candidate with one of the following final states: $e\mu$, $e\tau_h$, $\mu\tau_h$, or $\tau_h\tau_h$. The main irreducible backgrounds to the WH and ZH searches are WZ and ZZ diboson events, respectively. The irreducible backgrounds are estimated using simulation, corrected by control samples in data. The reducible backgrounds in both analyses are W, Z, and $t\bar{t}$ events with at least one quark or gluon jet misidentified as an isolated e, μ, or τ_h. These backgrounds are estimated solely from data by measuring the probability for jets to be misidentified as isolated leptons in background-enriched control regions, and weighting the selected events which fail the lepton requirements by the misidentification probability.

2.4 $H \to WW$

The $H \to WW^{(*)} \to 2\ell 2\nu$ analysis [76, 77] searches for an excess of events with two leptons of opposite charge, large E_T^{miss}, and up to two jets. Events are divided into six categories, with different background compositions and signal-to-background ratios. For events with no jets, the main background stems from non-resonant WW production; for events with one jet, the dominant backgrounds are from WW and top-quark production. The events are split into same-flavour and different-flavour dilepton sub-channels, since the background from Drell–Yan production is much larger for the same-flavour dilepton events. The two-jet category is optimized to take advantage of the VBF Higgs boson production signature. The main background in this channel is from top-quark production. In the 7 TeV analysis, the same-flavour and different-flavour categories with 2 jets are merged into one. To improve the separation of signal from backgrounds in the 7 TeV analysis, MVA classifiers are trained for a number of Higgs boson masses. The search is made for an excess of events in the output distributions of the classifiers. Similarly, in the 8 TeV analysis the bidimensional distribution of events in the $(m_{\ell\ell}, m_T)$ plane is used for different-flavour dilepton channels with zero and one jet; $m_{\ell\ell}$ is the invariant mass of the dilepton pair, and m_T is the transverse mass reconstructed from the transverse momentum of the dilepton and the missing transverse momentum. All background rates, except for very small contributions from WZ, ZZ, and Wγ, are evaluated from data.

The $H \to WW \to \ell\nu 2q$ analysis [74, 75] searches for an excess of events with one lepton (e or μ), E_T^{miss}, and two or three jets. Events are divided into four categories: e or μ and 2 or 3 jets. In all cases, the dominant background is W + jets. Because of the limited MC statistics for this background, a data-driven method is employed that models W + jets in the signal region from the dijet invariant mass sidebands. Smaller backgrounds include $t\bar{t}$, single top, diboson production (irreducible), and Z + jets, which are modeled from MC, and multijet production (electron channels only) which is estimated from data. Because only one neutrino is produced in this channel, both W bosons can be reconstructed, and a four-body mass peak for WW and WZ can be seen. A kinematic fit in which the lepton-missing-transverse-energy system is constrained to the on-shell W mass is performed to improve the resolution and reduce the background. To improve further the separation of signal from backgrounds, MVA classifiers that include the Higgs boson decay angles, the four-body rapidity and the p_T are built separately for each simulated Higgs mass point, for each of the four channels. Events passing an optimized cut on the MVA output are retained and a search is made for an excess of events in the four-body invariant mass distributions.

The $WH \to WWW \to 3\ell 3\nu$ analysis [78] searches for an excess of events with three leptons, electrons or muons, large missing transverse energy, and low hadronic activity. The dominant background is from $WZ \to 3\ell\nu$ production, which is largely reduced by requiring that all same-flavour oppositely charged lepton pairs have a dilepton mass away from m_Z. In addition, oppositely charged leptons are required not to be back-to-back. The background processes with jets misidentified as leptons, e.g. Z + jets and top, as well as the $WZ \to 3\ell\nu$ background are

estimated from data. The small contribution from the $ZZ \to 4\ell$ process with one of the lepton having escaped detection is estimated using simulated samples.

2.5 $H \to ZZ$

In the $H \to ZZ^{(*)} \to 4\ell$ channel [79], we search for a four-lepton mass peak over a small continuum background. To further separate signal and background, we use a discriminant calculated for each event as the ratio of the probabilities for signal and background to form an event with the observed kinematics (the masses of the dilepton pairs and the five angles fully defining a four-lepton configuration in their center-of-mass frame). The 4e, 4μ and $2e2\mu$ sub-channels are analysed separately since there are differences in the four-lepton mass resolutions and the background rates arising from jets misidentified as leptons. The dominant irreducible background in this channel is from non-resonant ZZ production with both Z bosons decaying to either 2e, 2μ, or 2τ (with the taus decaying leptonically) and is estimated from simulation. The smaller reducible backgrounds with jets misidentified as leptons, e.g. $Z + \text{jets}$, are estimated from data.

In the $H \to ZZ \to 2\ell 2\tau$ search [79], one Z boson is required to be on-shell and to decay to a lepton pair (ee or $\mu\mu$). The other Z boson is required to decay through a $\tau\tau$ pair to one of the four final-state signatures $e\mu$, $e\tau_h$, $\mu\tau_h$, $\tau_h\tau_h$. Thus, eight exclusive sub-channels are defined. We search for a broad excess in the distribution of the dilepton-ditau mass, constructed from the visible products of the tau decays, neglecting the effect of the accompanying neutrinos. The dominant background is non-resonant ZZ production whose rate is estimated from simulation. The main sub-leading backgrounds with jets misidentified as τ leptons stem from $Z + \text{jets}$ (including ZW) and top-quark events. These backgrounds are estimated from data.

Table 1: Summary of the information on the analyses included in this combination. All final states are exclusive. Notations used are: $(jj)_{VBF}$ stands for a dijet pair consistent with the VBF topology (VBF-tag); $(jj)_V$ – dijet pair with an invariant mass consistent with coming from a W or Z dijet decay; V – W and Z bosons; SF dileptons – ee or $\mu\mu$ pairs (same flavour); DF dileptons – $e\mu$ pairs (different flavour). The column "H prod" indicates which production mechanism is targeted by an analysis; it does not imply 100% purity (e.g. analyses targeting VBF are expected to have 30%-50% of their signal events coming from gluon-gluon fusion). The main contribution in the untagged and inclusive categories is always gluon-gluon fusion. When two references are given, they refer to the 7 TeV and 8 TeV analyses, respectively. When one reference is given for an analysis using both 7 and 8 TeV data, the 7 TeV data have been re-analysed with improved analysis strategies and the new results may differ from the previously published results.

Analyses			No. of	m_H range	m_H	Lumi (fb^{-1})		Ref
H decay	H prod	Exclusive final states	channels	(GeV)	resolution	7 TeV	8 TeV	
$\gamma\gamma$	untagged	$\gamma\gamma$ (4 diphoton classes)	4	110–150	1-2%	5.1	5.3	[69]
	VBF-tag	$\gamma\gamma + (jj)_{VBF}$ (low or high m_{jj} for 8 TeV)	1 or 2	110–150	1-2%	5.1	5.3	[69]
bb	VH-tag	($\nu\nu$, ee, $\mu\mu$, $e\nu$, $\mu\nu$ with 2 b-jets)$\times$ (low or high p_T^V or loose b-tag)	10 or 13	110–135	10%	5.0	12.1	[70]
	ttH-tag	(ℓ with 4,5,$\geq$6 jets) $\times$ (3,$\geq$4 b-tags); (ℓ with 6 jets with 2 b-tags); ($\ell\ell$ with 2 or $\geq$3 b-tagged jets)	9	110–140		5.0	-	[71]
$H \to \tau\tau$	1-jet	($e\tau_h$, $\mu\tau_h$, $e\mu$, $\mu\mu$)$\times$ (low or high p_T^τ) and $\tau_h\tau_h$	9	110–145	20%	4.9	12.1	[72]
	VBF-tag	($e\tau_h$, $\mu\tau_h$, $e\mu$, $\mu\mu$, $\tau_h\tau_h$) + $(jj)_{VBF}$	5	110–145	20%	4.9	12.1	[72]
	ZH-tag	(ee, $\mu\mu$) $\times$ ($\tau_h\tau_h$, $e\tau_h$, $\mu\tau_h$, $e\mu$)	8	110–160		5.0	-	[73]
	WH-tag	$\tau_h ee$, $\tau_h\mu\mu$, $\tau_h e\mu$	3	110–140		4.9	-	[73]
$WW \to \ell\nu qq$	untagged	($e\nu$, $\mu\nu$)$\times$($(jj)_W$ with 0 or 1 jets)	4	170–600		5.0	12.1	[74, 75]
$WW \to \ell\nu\ell\nu$	0/1-jets	(DF or SF dileptons) $\times$ (0 or 1 jets)	4	110–600	20%	4.9	12.1	[76, 77]
$WW \to \ell\nu\ell\nu$	VBF-tag	$\ell\nu\ell\nu + (jj)_{VBF}$ (DF or SF dileptons for 8 TeV)	1 or 2	110–600	20%	4.9	12.1	[76, 77]
$WW \to \ell\nu\ell\nu$	WH-tag	$3\ell 3\nu$	1	110–200		4.9	5.1	[78]
$ZZ \to 4\ell$	inclusive	$4e$, 4μ, $2e2\mu$	3	110–1000	1-2%	5.0	12.2	[79]
$ZZ \to 2\ell 2\tau$	inclusive	(ee, $\mu\mu$) $\times$ ($\tau_h\tau_h$, $e\tau_h$, $\mu\tau_h$, $e\mu$)	8	180–1000	10-15%	5.0	12.2	[80]

Table 2: Summary of production mechanisms and decay channels explicitly targeted in the searches for a low mass Higgs boson ($m_{\mathrm{H}} < 145\,\mathrm{GeV}$). Untagged searches include gluon-gluon fusion $gg \to \mathrm{H}$ plus any phase space not covered by searches with explicit tags for enriching datasets with events from VBF, VH, and $t\bar{t}$H production. V stands for W or Z. None of the analyses targeting a particular production mechanism are 100% pure and all have an admixture, sometimes very substantial, of other production mechanisms.

	untagged	VBF-tag	VH-tag	$t\bar{t}$H-tag
$\mathrm{H} \to \gamma\gamma$	✓	✓		
$\mathrm{H} \to b\bar{b}$			✓	✓
$\mathrm{H} \to \tau\tau$	✓	✓	✓	
$\mathrm{H} \to WW$	✓	✓	✓	
$\mathrm{H} \to \mathrm{ZZ}$	✓			

3 Combination methodology

The combination of the Higgs boson searches requires simultaneous analysis of the data selected by all individual analyses, accounting for all statistical and systematic uncertainties and their correlations. The overall statistical methodology used in this combination was developed by the ATLAS and CMS Collaborations in the context of the LHC Higgs Combination Group. The description of the general methodology can be found in Refs. [87, 88]. Below we give concise definitions of statistical quantities we use for characterizing the outcome of the search. Results presented in this note are obtained using asymptotic formulae [89], including a few updates recently introduced in the RooStats package [90].

3.1 Characterising the absence of a signal: limits

For calculations of exclusion limits, we adopt the modified frequentist criterion $\mathrm{CL_s}$ [91, 92]. The chosen test statistic q, used to determine how signal- or background-like the data are, is based on the profile likelihood ratio. Systematic uncertainties are incorporated in the analysis via nuisance parameters and are treated according to the frequentist paradigm. The profile likelihood ratio is defined as

$$q_\mu \;=\; -2\,\ln\frac{\mathcal{L}(\mathrm{obs}\,|\,\mu\cdot s+b,\,\hat{\hat{\theta}}_\mu)}{\mathcal{L}(\mathrm{obs}\,|\,\hat{\mu}\cdot s+b,\,\hat{\theta})}, \tag{1}$$

where s stands for the signal expected under the SM Higgs hypothesis, μ is a signal strength modifier introduced to accommodate deviations from SM Higgs predictions, b stands for backgrounds, and θ are nuisance parameters describing systematic uncertainties ($\hat{\hat{\theta}}_\mu$ maximizes the likelihood in the numerator for a given μ, while $\hat{\mu}$ and $\hat{\theta}$ define the point at which the likelihood reaches its global maximum).

The ratio of probabilities to observe a value of the test statistic at least as large as the one observed in data, q_μ^{obs}, under the signal+background (μ·s+b) and background-only (b) hypotheses,

$$\mathrm{CL_s} = \frac{\mathrm{P}(q_\mu \geq q_\mu^{\mathrm{obs}}\,|\,\mu\cdot s+b)}{\mathrm{P}(q_\mu \geq q_\mu^{\mathrm{obs}}\,|\,b)} \;\leq \alpha, \tag{2}$$

is used as the criterion for excluding a signal strenght μ·s at the $1-\alpha$ confidence level.

3.2 Characterising an excess of events: p-values and significance

To quantify the presence of an excess of events over what is expected for the background, we use the test statistic where the likelihood appearing in the numerator is for the background-only hypothesis:

$$q_0 \;=\; -2\,\ln\frac{\mathcal{L}(\mathrm{obs}\,|\,b,\,\hat{\hat{\theta}}_0)}{\mathcal{L}(\mathrm{obs}\,|\,\hat{\mu}\cdot s+b,\,\hat{\theta})}, \tag{3}$$

The statistical significance Z of a signal-like excess is computed from the probability p_0

$$p_0 = \mathrm{P}(q_0 \geq q_0^{obs}\,|\,\mathrm{b}), \tag{4}$$

henceforth referred to as the p-value, using the one-sided Gaussian tail convention.

$$p_0 = \int_Z^{+\infty} \frac{1}{\sqrt{2\pi}} \exp(-x^2/2)\ \mathrm{d}x. \tag{5}$$

We remind the reader that very small p-values from these formal calculations should be interpreted with caution as the systematic biases and uncertainties in the underlying model are only known with finite precision.

3.3 Extracting signal model parameters

Signal model parameters a (the signal strength modifier μ can be one of them) are evaluated from a scan of the profile likelihood ratio $q(a)$:

$$q(a) = -2 \ln \frac{\mathcal{L}(\mathrm{obs} \,|\, s(a) + b,\, \hat{\theta}_a)}{\mathcal{L}(\mathrm{obs} \,|\, s(\hat{a}) + b,\, \hat{\theta})}, \tag{6}$$

The parameters $\hat{a}$ and $\hat{\theta}$ that maximize the likelihood, $\mathcal{L}(\mathrm{obs} \,|\, s(\hat{a}) + b,\, \hat{\theta}) = \mathcal{L}_{\max}$, are called the best-fit set. The 68% (95%) CL on a given parameter of interest a_i is evaluated from $q(a_i) = 1$ (3.84) with all other unconstrained model parameters treated in the same way as the nuisance parameters. The 2D 68% (95%) CL contours for pairs of parameters are derived from $q(a_i, a_j) = 2.3$ (6). One should keep in mind that boundaries of 2D confidence regions projected on either parameter axis are not identical to the 1D confidence interval for that parameter.

4 Results

In this section we present results obtained by combining information from the search channels described previously. The mass range explored in the combination is 110 – 1000 GeV. First, we show that the SM Higgs boson is excluded at 95% CL in the mass range up to 700 GeV, except for a small window near $m_{\mathrm{H}} \sim 125$ GeV, where a new boson was recently discovered. The statistical significance of the new boson is now $6.9\,\sigma$. Then, we proceed with measuring the mass of the new boson. Next, we evaluate the consistency of the data observed in the different search channels with the expectations for a SM Higgs boson with mass equal to the mass of the observed boson. Finally we test whether the new boson is a CP-even or CP-odd scalar (0^+ or 0^-).

4.1 Exclusion limits on the SM Higgs boson

The $\mathrm{CL_s}$ value for the SM Higgs boson hypothesis as a function of its mass is shown in Fig. 3. The observed values are shown by the solid line. The dashed black line indicates the median of the expected results for the background-only hypothesis, with the green (dark) and yellow (light) bands indicating the ranges in which the $\mathrm{CL_s}$ values are expected to reside in 68% and 95% of the experiments under the background-only hypothesis. The probabilities for an observation to lie above or below the 68% (95%) band are 16% (2.5%) each. The red horizontal lines indicate $\mathrm{CL_s}$ values of 0.05, 0.01, and 0.001. The mass regions where the observed $\mathrm{CL_s}$ values are below these lines are excluded with the corresponding $(1 - \mathrm{CL_s})$ confidence levels of 95%, 99%, and 99.9%, respectively. In the high mass region, we exclude a SM Higgs boson at 95% CL up to 700 GeV. In the low mass region the gap between 121 and 128 GeV is due to the recently discovered boson with a mass near 125 GeV. With the addition of more data and updates to the analyses the expected limit improves. However the observed limit is subject to statistical fluctuation, and indeed in this current combination a small 1-GeV wide segment around m_{H}= 113 GeV that was excluded in the two previous combinations [11, 93] is now above the 95% CL exclusion line.

Figure 4 shows the 95% CL upper limits on the signal strength modifier, $\mu = \sigma/\sigma_{\mathrm{SM}}$, as a

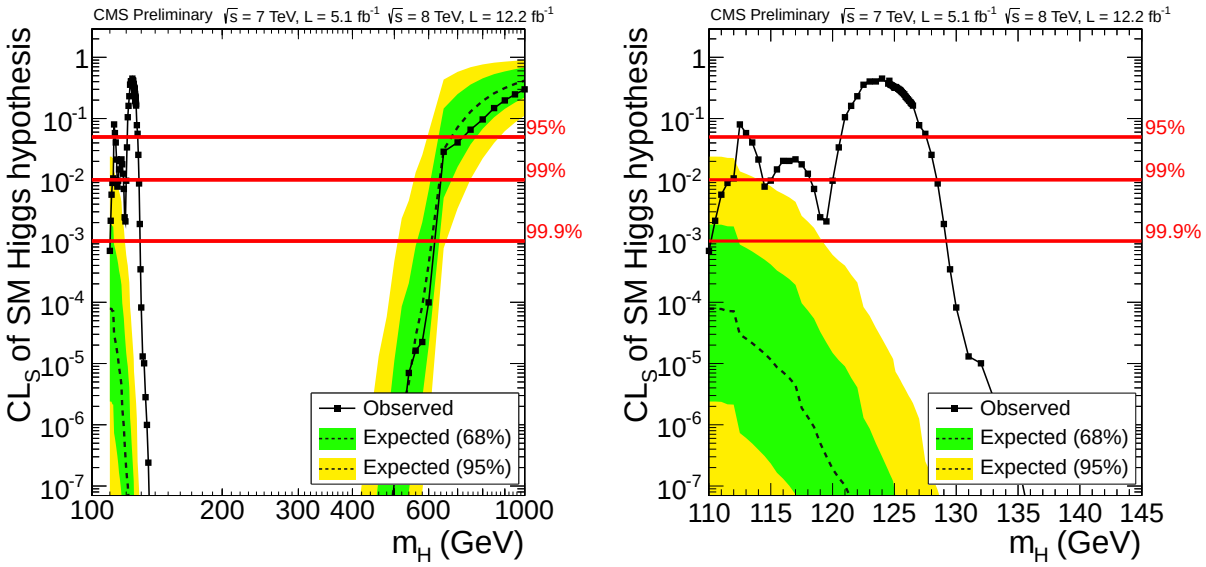

Figure 3: The $\mathrm{CL_s}$ values for the SM Higgs boson hypothesis as a function of the Higgs boson mass, in the range 110–1000 GeV (left) and 110–145 GeV (right). The background-only expectations are represented by their median (dashed line) and by the 68% and 95% CL bands.

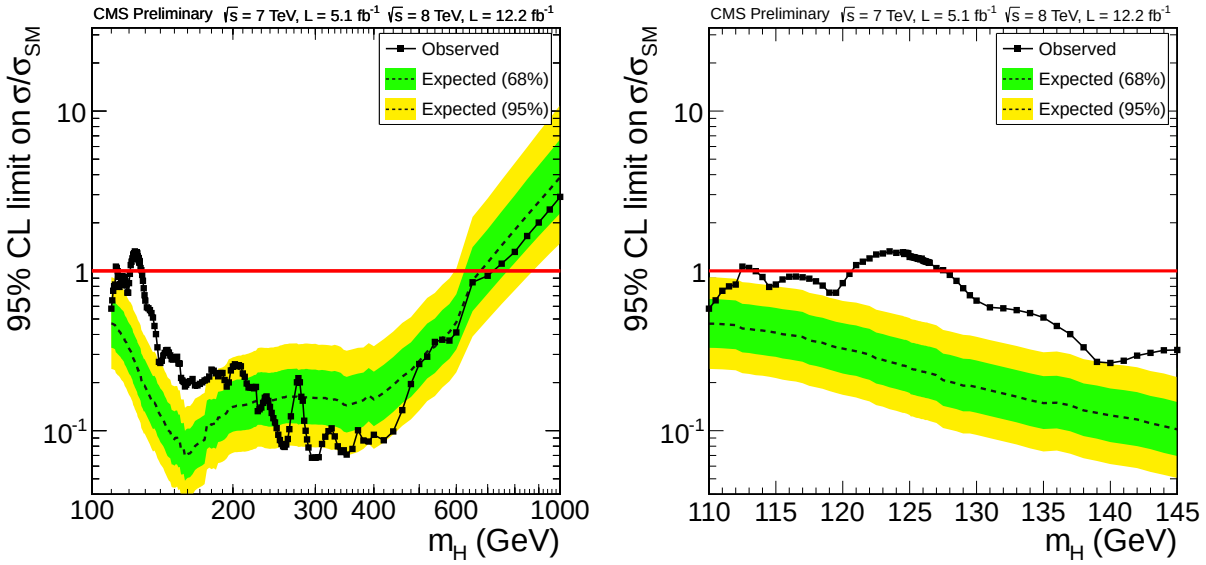

Figure 4: The 95% CL upper limits on the signal strength parameter, $\mu = \sigma/\sigma_{\mathrm{SM}}$, in the range 110–1000 GeV (left) and 110–145 GeV (right).

function of m_{H}. The ordinate thus shows the Higgs boson cross section that is excluded at 95% CL, expressed as a multiple of the SM Higgs boson cross section.

Figure 3 shows, that in the absence of a signal, we expect to exclude the range from 110–650 GeV at 95% CL. For $m_{\mathrm{H}} > 200$ GeV, the differences between the observed and expected limits are consistent with statistical fluctuations since the observed limits are generally within the green (68%) or yellow (95%) bands. The broad excess seen for $m_{\mathrm{H}} < 200$ GeV is attributed to the new boson with a mass near 125 GeV and is discussed in the next section.

4.2 Significance of the observed excess

To quantify the inconsistency of the observed excess with the background-only hypothesis, we show in Fig. 5 the local p-values for the various sub-combinations by decay channel and for the overall combination. With the dataset used in this combination, the new boson with a mass near 125 GeV has a significance of $6.9\,\sigma$. The mass corresponding to the largest significance is 125.8 GeV. However, this value should not be treated as a measurement of the mass of the new boson; this topic is presented in Section 4.3. Other than the new boson, we see no evidence for a significant excess of events that could be attributed to either an additional particle or particles. The largest contributors to the overall excess in the combination near the mass of 125 GeV are the $\mathrm{ZZ} \to 4\ell$ and $\gamma\gamma$ channels, with maximum significances of $4.4\,\sigma$ and $4.0\,\sigma$. The WW channel contributes about $3\,\sigma$, and the bb and $\tau\tau$ contribute about $2\,\sigma$ each. The excess in the WW channel extends up to about 200 GeV, as a consequence of the 125-GeV boson and a modest (about $1\,\sigma$) upward fluctuation in the background. The expected significance in this channel reaches $\approx 3\,\sigma$ in a broad m_{H} range up to 150 GeV, as shown in the right-hand plot of Fig.12 of Ref. [77]. This causes a second minimum reaching about 4σ around 145 GeV, when combined with a few events in excess from the ZZ channel.

Many of the nuisance parameters describing the systematic uncertainties are constrained by the data in the different regions of phase space relevant for particular Higgs boson mass hypotheses. This process leads to small irregular variations in the expected p-value vs m_{H}.

The $\gamma\gamma$ and $\mathrm{ZZ} \to 4\ell$ channels are characterised by their very good mass resolution, allowing the invariant mass of the observed resonance to be well localized. Their combined significance

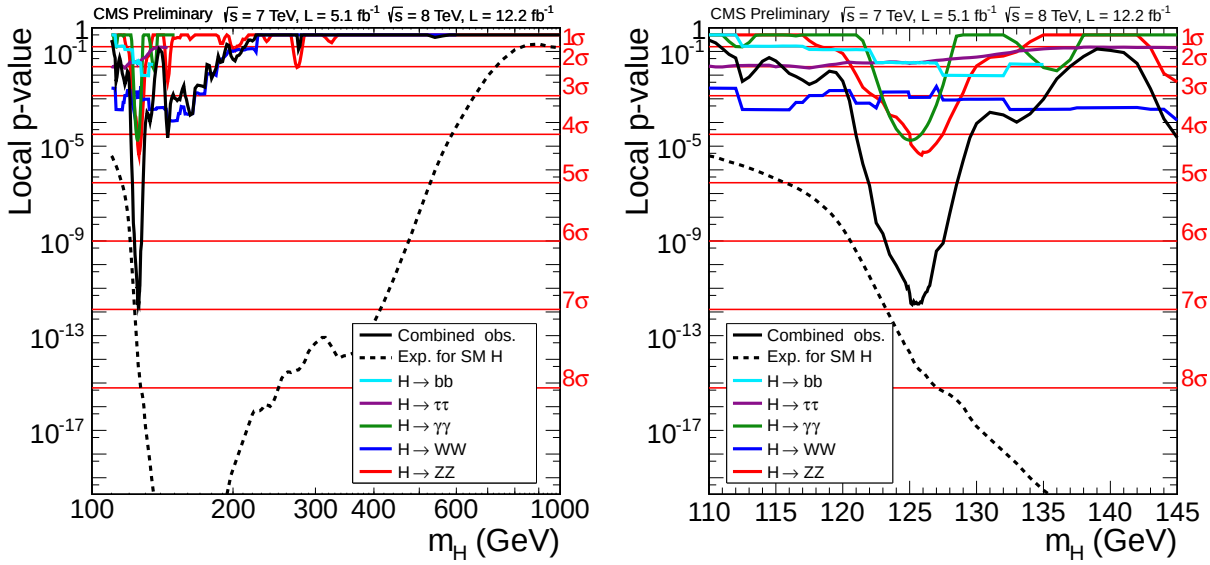

Figure 5: The observed local p-value for the five decay mode and the overall combination as a function of the SM Higgs boson mass in the range 110–1000 GeV (left) and 110–145 GeV (right). The dashed lines show the expected local p-values for a SM Higgs boson with a mass m_{H}.

reaches 5.8 σ, as can be seen in Fig. 6 (left). Figure 6 (right) shows the combination for the channels with poor mass resolution, namely: WW, bb, and $\tau\tau$. The jagged behaviour is due to analyses that consider different Higgs boson mass hypotheses in steps proportional to the mass resolution of that channel.

Table 3 summarises the median expected and observed local significances for a SM Higgs boson mass hypothesis of 125.8 GeV for the individual decay modes and their various combinations. The median expected significance is evaluated for a pseudo-observation equal to the median expected background plus signal rate. The ± 1 range around the median significance should contain 68% of the statistical fluctuations that could occur in data.

Table 3: The significance of the median expected and observed event excesses in individual decay modes and their various combinations for a SM Higgs boson mass hypothesis of 125.8 GeV. The expected range of possible statistical deviations from the median expected significance is about ± 1.

Decay mode or combination	Expected (σ)	Observed (σ)
ZZ	5.0	4.4
$\gamma\gamma$	2.8	4.0
WW	4.3	3.0
bb	2.2	1.8
$\tau\tau$	2.1	1.8
$\gamma\gamma$ + ZZ	5.7	5.8
$\gamma\gamma$ + ZZ + WW + $\tau\tau$ + bb	7.8	6.9

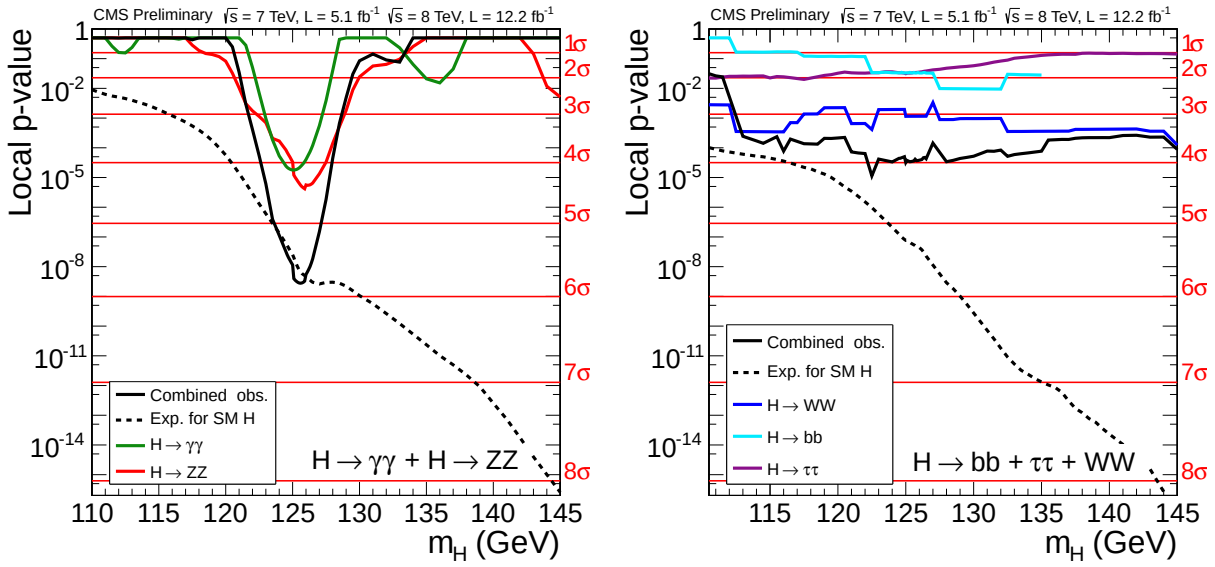

Figure 6: The observed local p-value for decay modes with high mass-resolution channels (left), $\gamma\gamma$ and ZZ, and low mass-resolution (right) as a function of the SM Higgs boson mass. The dashed lines show the expected local p-values for a SM Higgs boson with a mass m_{H}.

4.3 Mass of the observed state

To measure the mass of the observed state, we use the ZZ $\to 4\ell$ and $\gamma\gamma$ channels that have excellent mass resolution (Table 1) and for which we observe excesses with significances of $4.4\,\sigma$ and $4.0\,\sigma$, respectively. Figure 7 (left) shows 2D 68% confidence level regions for the two parameters of interest, the signal strength modifier μ and the mass m_X, for these channels. The combined 68% CL contour shown with a black line in Fig. 7 (left) fixes the relative event yield between the two channels to the SM Higgs boson expectation, while the overall signal strength is left as a free parameter.

To extract the value of m_X in a model-independent way, the signal strength modifiers for the $gg \to \mathrm{H} \to \gamma\gamma$, VBF+VH$\to \gamma\gamma$, and $\mathrm{H} \to \mathrm{ZZ} \to 4\ell$ processes are assumed to be independent and, thus, not tied to the SM expectation. The signal in all channels is assumed to be due to a state with a unique mass, m_X. The mass m_X and its uncertainty are extracted from a scan of the combined test statistic $q(m_X)$ with the three signal strength modifiers profiled in the same way as all other nuisance parameters. Figure 7 (right) shows the scan of the test statistic as a function of the hypothesised mass m_X for the two final states separately and their combination. Crossings of the $q(m_X)$ curves with the horizontal thick (thin) lines at 1 (3.8) define the 68% (95%) CL intervals for the mass of the observed particle. These intervals include both statistical and systematic uncertainties. The 68% CL interval is m_X =125.8 $\pm$ 0.5 GeV.

To evaluate the statistical component of the overall error, we also perform a scan of the test statistic $q(m_X)$ with all nuisance parameters fixed to their best-fit values. The result is shown by the dashed line in Fig. 8. The crossings of the dashed line with the thick horizontal line define the statistical error (68% CL interval) in the mass measurement: $m_X = 125.8 \pm 0.4$ (stat.) GeV. Assuming that the total error is the sum in quadrature of the statistical and systematic compo-

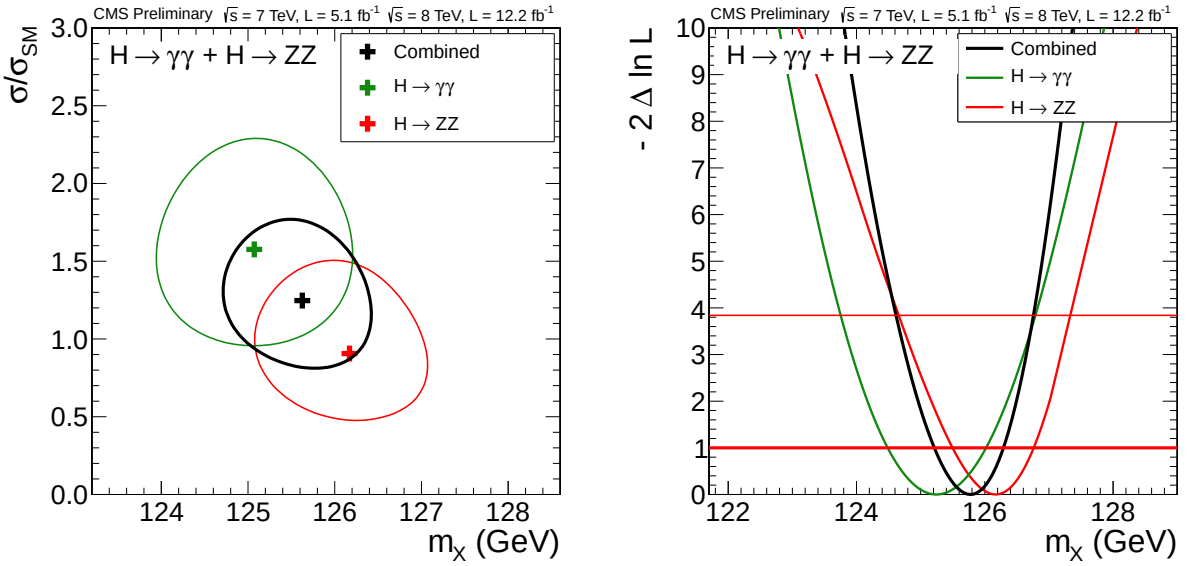

Figure 7: (Left) The 68% CL contours for the signal strength $\sigma/\sigma_{\mathrm{SM}}$ versus the boson mass m_X for the $\gamma\gamma$ and 4ℓ final states, and their combination. The symbol $\sigma/\sigma_{\mathrm{SM}}$ denotes the production cross section times the relevant branching fractions, relative to the SM expectation. In this combination, the relative signal strength for the two decay modes are constrained by the expectations for the SM Higgs boson. (Right) 1D-scan of the test statistic $q(m_X)$ (or $-2\,\Delta \ln L$) vs the boson mass m_X for the $\gamma\gamma$ and 4ℓ final states separately and for their combination. In this combination the two independent signal strengths, $gg \to \mathrm{H} \to \gamma\gamma$, and $\mathrm{H} \to \mathrm{ZZ} \to 4\ell$, are profiled together with all other nuisance parameters.

nents, we extract a systematic error of ± 0.4 GeV. Therefore, the final mass measurement can be written as $m_X = 125.8 \pm 0.4\,(\text{stat}) \pm 0.4\,(\text{syst})$ GeV.

To assess the dependency of the mass measurement on the SM Higgs boson hypothesis, the measurement is repeated using the same channels but constraining instead all production cross sections and branching ratios to the SM predictions as function of m_H. The two results are compatible to better than 0.1 GeV, both with respect to the central value and the uncertainties.

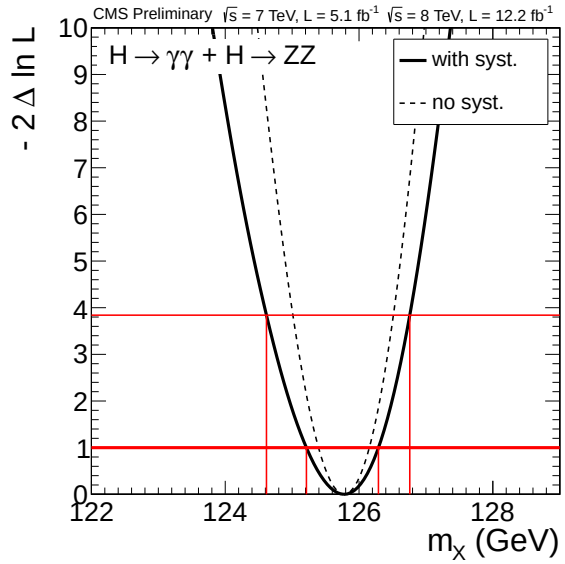

Figure 8: 1D-scans of the test statistic $q(m_X)$ versus the boson mass m_X for the combination of the $\gamma\gamma$ and 4ℓ final states. The solid line is obtained with all nuisance parameters profiled and, hence, includes both statistical and systematic uncertainties. The dashed line is obtained with all nuisance parameters fixed to their best-fit values and, hence, includes only statistical uncertainties. The crossings with the thick (thin) horizontal lines define the 68% (95%) CL interval for the measured mass.

4.4 Compatibility of the observed state with the SM Higgs boson hypothesis

The p-values characterise the probability of background producing the observed excesses, but they do not give information about the compatibility of the observed excesses with the expected signal. The size of the current data set only allows a limited number of such tests, which we present in this subsection. These compatibility tests do not constitute measurements of any physics parameters per se, but rather show the consistency of the various observations with the expectations for the SM Higgs boson.

4.4.1 Signal strength in combination and sub-combinations

The best fit value for the common signal strength modifier $\hat{\mu} = \sigma/\sigma_{\text{SM}}$, obtained in the combination of all search channels, provides the first compatibility test. In the formal fit, $\hat{\mu}$ is allowed to become negative if the observed number of events is smaller than the expected rate for the background-only hypothesis. Figure 9 shows a scan of the $\hat{\mu}$ value versus the hypothesised Higgs boson mass m_H. The band corresponds to the $\pm 1\sigma$ uncertainty (statistical+systematic). The observed $\hat{\mu}$ value for a hypothesised Higgs boson mass of 125.8 GeV is found to be 0.88 ± 0.21 and is consistent with the value expected for the SM Higgs boson ($\mu = 1$) within the $\pm 1\sigma$ uncertainties.

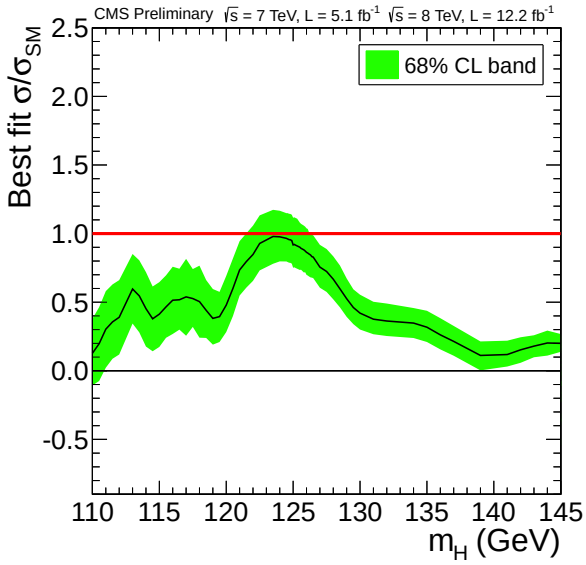

Figure 9: The observed best-fit signal strength, $\sigma/\sigma_{\mathrm{SM}}$, as a function of the SM Higgs boson mass m_{H} in the range 110–145 GeV for the combined 7 and 8 TeV data sets. The symbol $\sigma/\sigma_{\mathrm{SM}}$ denotes the production cross section times the relevant branching fractions, relative to the SM expectation. The band corresponds to the ± 1 standard deviation uncertainty in $\sigma/\sigma_{\mathrm{SM}}$.

Figure 10 shows the $\hat{\mu}$ values obtained in different sub-combinations of search channels for m_{H}= 125.8 GeV, organized by decay mode and by additional tags used to select preferentially events from a particular production mechanism. The expected purities of the different tagged samples vary substantially. For example, assuming the SM Higgs boson cross sections, the channels with the di-jet VBF tag always have a substantial fraction (20-50%) of gluon-gluon fusion events. Therefore, these compatibility plots must not be interpreted literally as compatibility tests for pure production mechanisms and decay modes.

The plots show a satisfactory level of compatibility between all the channels contributing to the combination. None of the sub-combinations depart from the SM Higgs boson hypothesis, $\mu = 1$, by a significant deviation with respect to their current individual sensitivities. The level of compatibility of any sub-combination with the SM Higgs boson cross section can be characterized by the value of the test statistic

$$q_\mu = -2\,\Delta \ln \mathcal{L} = -2\,\ln \frac{\mathcal{L}(\mathrm{data}\,|\,\mu, \hat{\theta}_\mu)}{\mathcal{L}(\mathrm{data}\,|\,\hat{\mu}, \hat{\theta})} \tag{7}$$

at $\mu = 1$, which, asymptotically in the limit of large statistics, has a χ^2 distribution. For N sub-combinations, the sum of the individual $q_\mu(\mu = 1)$ values is expected to behave asymptotically as a χ^2 distribution with N degrees of freedom. In addition to the asymptotic p-value corresponding to the obtained $-2\,\Delta \ln \mathcal{L}$ value, we assess the true p-value by generating pseudo-observations. This procedure allows one to take into account that some channels may still have a very low event count and the presence of systematic uncertainties and their correlations.

The 11 sub-channel combination shown in Fig. 10 (top) gives a $\chi^2/\mathrm{n.d.f.} = 8.7/11$, which corresponds to an asymptotic p-value of 0.65. The p-value obtained by generating a large number of pseudo-experiments is 0.46. The 5 sub-combinations by decay mode shown in Figure 10 (bottom-left) give a $\chi^2/\mathrm{n.d.f.} = 4.3/5$, an asymptotic p-value of 0.51 and a p-value from pseudo-experiments of 0.54. Figure 10 (bottom-right) gives a $\chi^2/\mathrm{n.d.f.} = 1.3/4$, an asymptotic p-value=0.86 and a p-value from pseudo-experiments of 0.87. These numbers indicate that

the extracted signal strengths in these sub-combinations provide no evidence against the SM prediction for the Higgs boson ($\mu = 1$).

The four main Higgs boson production mechanisms can be associated with either top-quark couplings (gluon-gluon fusion and ttH) or vector boson couplings (VBF and VH). Therefore, a combination of channels associated with a particular decay mode and explicitly targeting different production mechanisms, can be used to test the relative strengths of the couplings to the vector bosons and the top quark. Figure 11 shows 68% CL intervals for the signal strength modifiers associated with the gluon-gluon-fusion-plus-ttH and for VBF-plus-VH production mechanisms, $\mu_{gg+\mathrm{ttH}}$ and $\mu_{\mathrm{VBF+VH}}$, respectively. The three sets of contours correspond to the five combinations by decay mode. In the $\mathrm{ZZ} \to 4\ell$ analysis, the different production mechanisms are not yet explicitly targeted; hence the range allowed by this channel becomes a diagonal strip. In all other channels, the different production mechanisms are explicitly exploited, leading to elliptical allowed regions. The SM Higgs boson point (1,1) is within the 95% CL intervals for each of these channels.

4.4.2 Compatibility of the observed data with the SM Higgs boson couplings

The event yield in any (production)×(decay) mode is related to the partial and total Higgs boson decay widths via the following equation:

$$N(xx \to \mathrm{H} \to yy) \sim \sigma(xx \to \mathrm{H}) \cdot \mathcal{B}(\mathrm{H} \to yy) \sim \frac{\Gamma_{xx}\,\Gamma_{yy}}{\Gamma_{\mathrm{tot}}}. \tag{8}$$

Eight parameters, namely the seven partial widths (Γ_{WW}, Γ_{ZZ}, Γ_{tt}, Γ_{bb}, $\Gamma_{\tau\tau}$, Γ_{gg}, $\Gamma_{\gamma\gamma}$) and the total width (Γ_{tot}) are relevant for the current searches. The partial widths, Γ_{gg} and $\Gamma_{\gamma\gamma}$, are generated by loop diagrams and are directly sensitive to the presence of new physics. The possibility of Higgs boson decays to beyond-standard-model (BSM) particles, with a partial width Γ_{BSM}, is accommodated by keeping Γ_{tot} as an independent parameter so that $\Gamma_{\mathrm{tot}} = \sum \Gamma_{i(\mathrm{SM})} + \Gamma_{\mathrm{BSM}}$, where $\Gamma_{i(\mathrm{SM})}$ stands for the partial widths of decays to SM particles. The partial widths are proportional to the square of the effective Higgs boson couplings to the corresponding particles. To test for possible deviations in the data from the rates expected in the different channels for the SM Higgs boson, we introduce modified couplings, denoted by scale factors κ_i and fit the data to these new parameters. Here i can stand for: v (vector boson), w (W boson), z (Z boson), f (fermions), l (leptons), q (quarks), u (up type leptons and quarks), d (down type lepton and quarks), b (b quark), t (top quark), τ, g (gluons, i.e. not resolving the loop), γ (photons, i.e. not resolving the loop). Significant deviations of the κ's from unity would imply new physics beyond the SM Higgs boson hypothesis. In this note we follow the prescriptions of the LHC Higgs Cross Section Working Group [94].

The size of the current dataset is insufficient to quantify meaningfully all eight phenomenological parameters defining the Higgs boson production and decay rates. Therefore, we present a number of combinations with a more limited number of degrees of freedom. The remaining unmeasured degrees of freedom are either constrained to be equal to the SM Higgs boson expectations or profiled in the likelihood scans together with all other nuisance parameters.

Test of the custodial symmetry

In the SM, the Higgs sector possesses a global $\mathrm{SU}(2)_{\mathrm{L}} \times \mathrm{SU}(2)_{\mathrm{R}}$ symmetry, which is broken by the Higgs vacuum expectation value down to the diagonal subgroup $\mathrm{SU}(2)_{\mathrm{L+R}}$. As a result, the tree-level relations between the W and Z masses, $m_{\mathrm{w}}/m_{\mathrm{z}}$, and their couplings to the Higgs boson, $g_{\mathrm{w}}/g_{\mathrm{z}}$, are protected against large radiative corrections, a property known as "custodial

symmetry" [95]. However, large violations of custodial symmetry are possible in new physics models. To test the custodial symmetry, we introduce two scaling factors κ_{w} and κ_{z} that modify the SM Higgs boson couplings to the W and Z bosons and perform two combinations to assess the consistency of the ratio $\lambda_{\mathrm{wz}} = \kappa_{\mathrm{w}}/\kappa_{\mathrm{z}}$ with unity.

The dominant production mechanism populating the inclusive $pp \to \mathrm{H} \to \mathrm{ZZ}$ and untagged $pp \to \mathrm{H} \to \mathrm{WW}$ search channels is $gg \to \mathrm{H}$. Therefore, the ratio of event yields in these channels provides a nearly model independent measurement of λ_{wz}. To properly account for the small unequal fractions of the VBF component in the two channels, we perform a combination of these two channels with two free parameters, κ_{z} and λ_{wz}. The likelihood scan vs λ_{wz} is shown in Fig. 12 (left). The scale factor κ_{z} is treated as a nuisance parameter, and κ_f kept =1. The 95% CL interval for λ_{wz} is [0.57,1.65] and, hence, the data are consistent with the expectation ($\lambda_{\mathrm{wz}} = 1$).

Alternatively, we extract λ_{wz} explicitly from the overall combination of all channels. In this approach, we introduce three degrees of freedom: λ_{wz}, κ_{z}, and κ_f. The last factor is a single modifier for all Higgs boson couplings to fermions. The BSM Higgs boson width Γ_{BSM} is set to zero. The partial width Γ_{gg}, induced by the quark loops, scales as κ_f^2. The partial width $\Gamma_{\gamma\gamma}$ is induced via loop diagrams, with the W boson and top quark being the dominant contributors; hence, it scales as $|\alpha\,\kappa_{\mathrm{w}} + \beta\,\kappa_f|^2$, where $\kappa_{\mathrm{w}} = \lambda_{\mathrm{wz}} \cdot \kappa_{\mathrm{z}}$ and the factors α and β are taken from predictions for the SM Higgs boson [26] (for $m_{\mathrm{H}} = 125.8$ GeV, $\beta/\alpha \sim -0.22$). In the likelihood scan $q(\lambda_{\mathrm{wz}})$, both κ_{z} and κ_f are profiled together with all other nuisance parameters. The introduction of one common scaling factor for all fermions makes this measurement model-dependent, but using all channels gives it greater statistical power. The likelihood scan is shown in Fig. 12 (right) with a solid line. The dashed line indicates the median expected result for the SM Higgs boson, given the current dataset. The 95% CL interval for λ_{wz} obtained in a combination of all channels is [0.67,1.55] and, hence, the data agree with the expectation set by the custodial symmetry.

In all combinations presented further, we assume $\lambda_{\mathrm{wz}} = 1$ and use a common factor κ_{v} to modify the couplings to W and Z bosons, whilst preserving their ratio.

Test of couplings to the vector bosons and fermions

An initial comparison of the observation with the expectation for the standard model Higgs boson is to fit for the two parameters, κ_{v} and κ_f, as defined previously. We assume that $\Gamma_{\mathrm{BSM}} = 0$, i.e. no new Higgs boson decay modes are open. At LO, all partial widths, except for $\Gamma_{\gamma\gamma}$, scale either as κ_{v}^2 or κ_f^2. As discussed before, the partial width $\Gamma_{\gamma\gamma}$ is induced via W and top loop diagrams and scales as $|\alpha\,\kappa_{\mathrm{v}} + \beta\,\kappa_f|^2$. Hence, the $\gamma\gamma$ channel is the only channel that is sensitive to the relative sign of κ_{v} and κ_f.

Figure 13 shows the 2D likelihood scan over the (κ_{v}, κ_f) phase space. The left plot allows for different signs of κ_{v} and κ_f, while the right plot constrains the phase space to the quadrant (+,+). The 68%, 95% and 99.7% confidence regions for κ_{v} and κ_f are shown with solid, dashed and dotted lines, respectively. The difference between the global minimum in (+,−) quadrant and the local minimum in the (+,+) quadrant is not statistically significant. The fact that the global minimum is in the quadrant (+,−) is driven by the excess in the $\gamma\gamma$ channel. If the relative sign between κ_{v} and κ_f is negative, the destructive interference between W and top-quark loops responsible for the $\mathrm{H} \to \gamma\gamma$ decays becomes positive and helps boost the decay branching fraction. The data are compatible with the expectation for the standard model Higgs boson: the point (κ_V, κ_F)=(1,1) is within the 95% confidence interval defined by the data. By the nature of the way these compatibility tests are constructed, any significant deviations from

(1,1), should they be observed, do not have straightforward interpretations within the SM and imply BSM physics; the scale/sign of the best-fit values in such an eventuality would guide us toward identifying the most plausible BSM scenarios. Figure 14 shows the interplay of different decay modes. The 95% CL intervals for κ_V and κ_F are each obtained from a 1D scan where the other parameter is fixed to unity, and equal [0.78,1.19] and [0.40,1.12], respectively.

Test for presence of BSM particles

The presence of BSM physics can considerably modify the Higgs boson phenomenology even if the underlying Higgs boson sector in the model remains unaltered. Processes induced by loop diagrams ($H \to \gamma\gamma$ and $gg \to H$) can be particularly susceptible to the presence of new particles. Therefore, we combine and fit the data for the scale factors (κ_γ and κ_g) for these two processes. The partial widths associated with the tree-level production processes and decay modes are assumed to be unaltered.

Figure 15 shows the 2D likelihood scan for the κ_g and κ_γ parameters (assuming $\Gamma_{\text{BSM}} = 0$). The results are compatible with the expectation for the SM Higgs boson as the point $(\kappa_\gamma, \kappa_g) = (1, 1)$ is within the 95% CL region defined by the data. The best-fit value is $(\kappa_\gamma, \kappa_g) = (1.43, 0.81)$, while the 95% CL intervals for each of these couplings separately are [0.98,1.92] for κ_γ and [0.55,1.07] for κ_g.

Figure 16 shows the likelihood scan versus $\text{BR}_{\text{BSM}} = \Gamma_{\text{BSM}}/\Gamma_{\text{tot}}$, with κ_g and κ_γ profiled together with all other nuisance parameters. The data allow us to conclude that BR_{BSM} is in the interval [0.00,0.62] at 95% CL.

Test for asymmetries in couplings to fermions

In models with two Higgs doublets (2HDM), the couplings of the neutral Higgs bosons to fermions can be substantially modified with respect to the Yukawa couplings of the SM Higgs boson. For example, in the MSSM, the couplings of neutral Higgs bosons to up-type and down-type fermions are modified, with the modification being the same for all three generations and for quarks and leptons. In more general 2HDMs, leptons can be made to virtually decouple from the Higgs boson that otherwise behaves in a SM-like way with respect to W/Z-bosons and quarks. Inspired by the possibility of such modifications to the fermion couplings, we perform two combinations, in which we allow for different ratios of the couplings to down/up fermions ($\lambda_{\text{du}} = \kappa_{\text{d}}/\kappa_{\text{u}}$) or different ratios of couplings to lepton and quarks ($\lambda_{\ell\text{q}} = \kappa_\ell/\kappa_{\text{q}}$). We assume that $\Gamma_{\text{BSM}} = 0$.

Figure 17 (left) shows the likelihood scan vs λ_{du}, with κ_{v} and κ_{u} profiled together with all other nuisance parameters. Figure 17 (right) shows the likelihood scan vs $\lambda_{\ell\text{q}}$, with κ_{v} and κ_{q} profiled. Both λ_{du} and $\lambda_{\ell\text{q}}$ are constrained to be positive; the 95% CL intervals for them are [0.45,1.66] and [0.00,2.11] respectively.

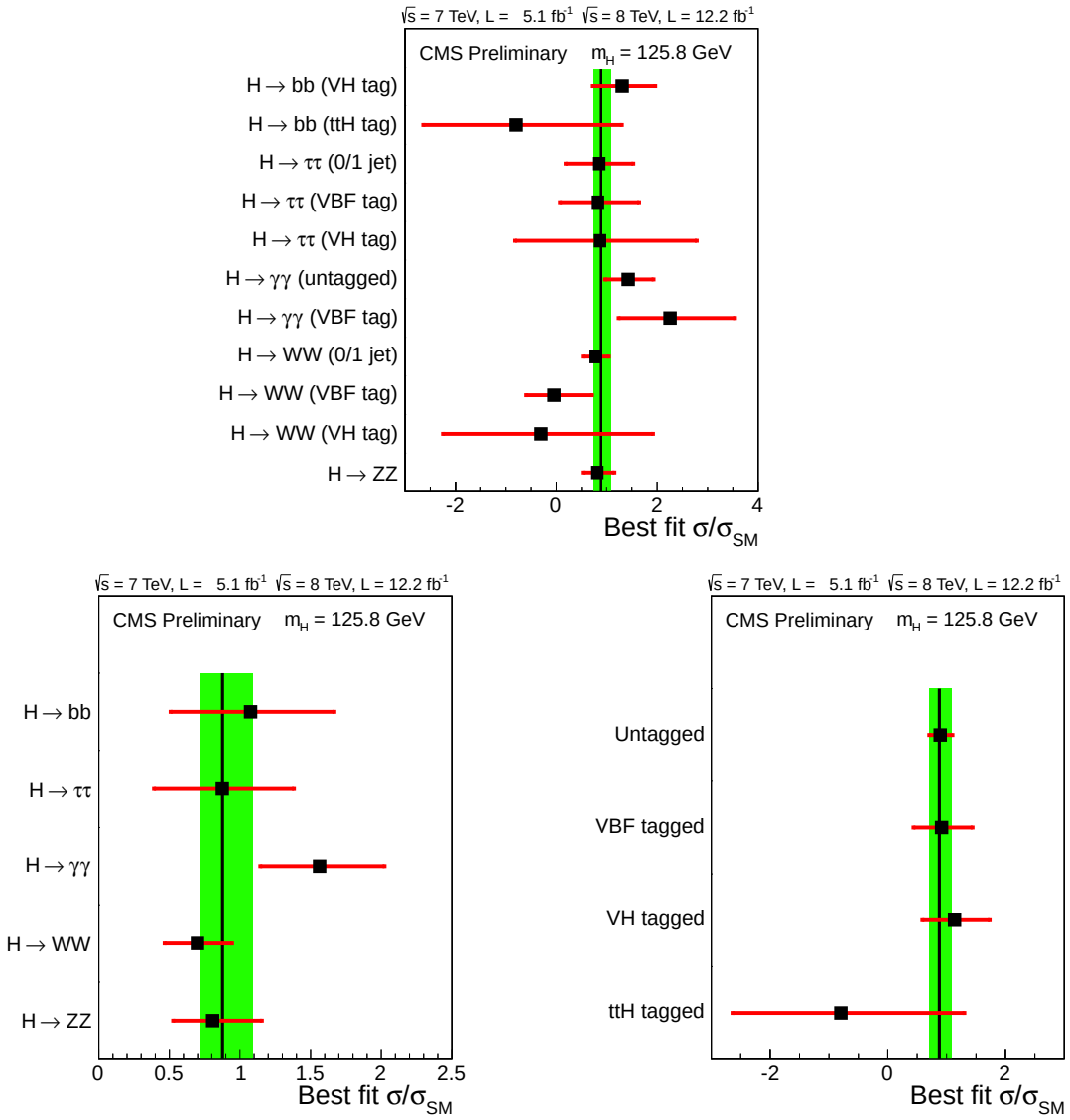

Figure 10: Values of $\sigma/\sigma_{\mathrm{SM}}$ for the combination (solid vertical line), for individual decay modes (point) or sub-combinations of decay modes. The vertical band shows the overal $\sigma/\sigma_{\mathrm{SM}}$ uncertainty. The symbol $\sigma/\sigma_{\mathrm{SM}}$ denotes the production cross section times the relevant branching fractions, relative to the SM expectation. The horizontal bars indicate the ± 1 standard deviation uncertainties in the $\sigma/\sigma_{\mathrm{SM}}$ values for the individual modes; they include both statistical and systematic uncertainty. (Top) Sub-combinations by decay mode and by additional tags targeting a particular production mechanism. (Bottom-left) Sub-combinations by decay mode. (Bottom-right) Sub-combinations by targeted production mechanism.

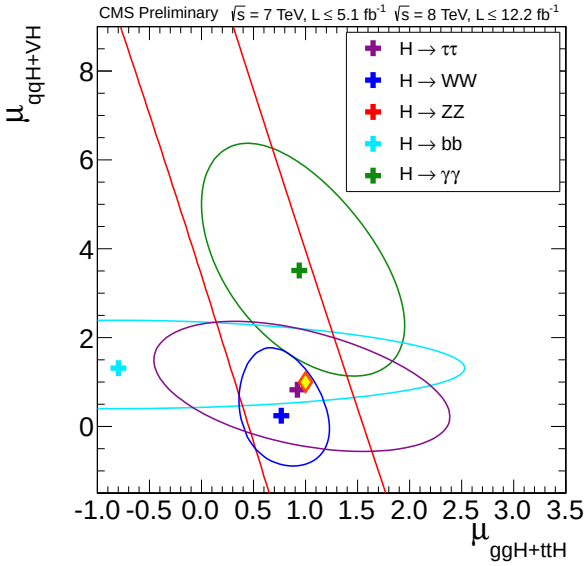

Figure 11: The 68% (solid lines) CL ranges for the signal strength in the gluon-gluon-fusion-plus-ttH and in VBF-plus-VH production mechanisms, $\mu_{gg+\mathrm{ttH}}$ and $\mu_{\mathrm{VBF+VH}}$, respectively. The different colors show the results obtained by combining data from each of the five analysed decay modes: $\gamma\gamma$ (green), WW (blue), ZZ (red), $\tau\tau$ (violet), bb (cyan). The crosses indicate the best-fit values. The diamond at (1,1) indicates the expected values for the SM Higgs boson.

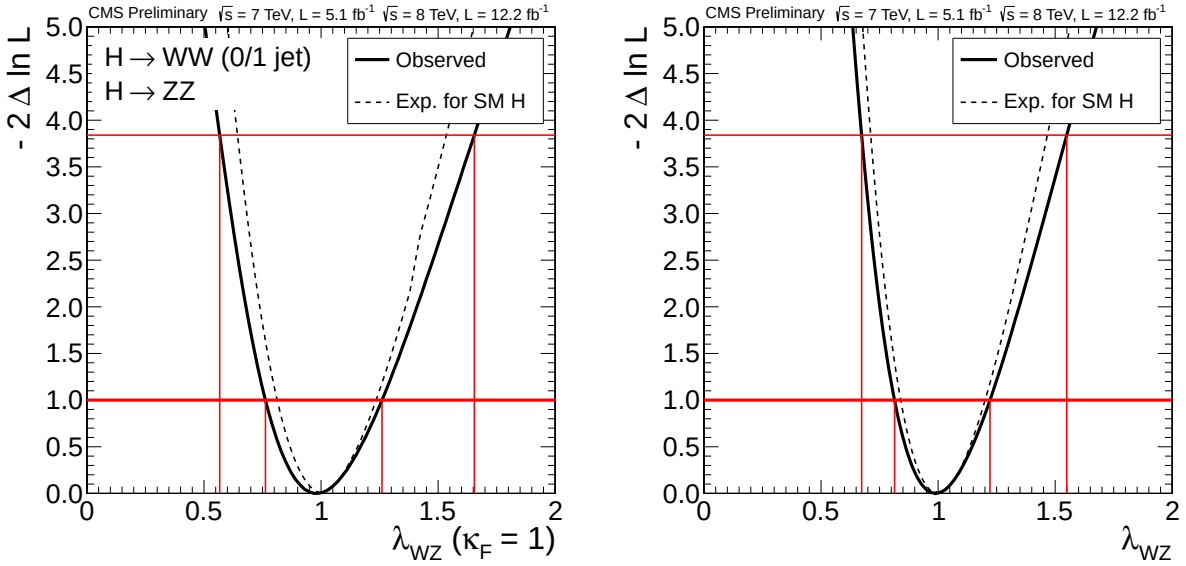

Figure 12: Likelihood scan vs λ_{WZ}, the ratio of the couplings to W and Z bosons. (Left) from untagged $pp \to \mathrm{H} \to \mathrm{WW}$ and inclusive $pp \to \mathrm{H} \to \mathrm{ZZ}$ searches, and assuming SM couplings to fermions. (Right) from the combination of all channels, profiling the coupling to fermions. The solid curve is the data. The dashed line indicates the expected median results in the presence of the SM Higgs boson. Crossings with the horizontal thick and thin red lines denote the 68% CL and 95% CL intervals.

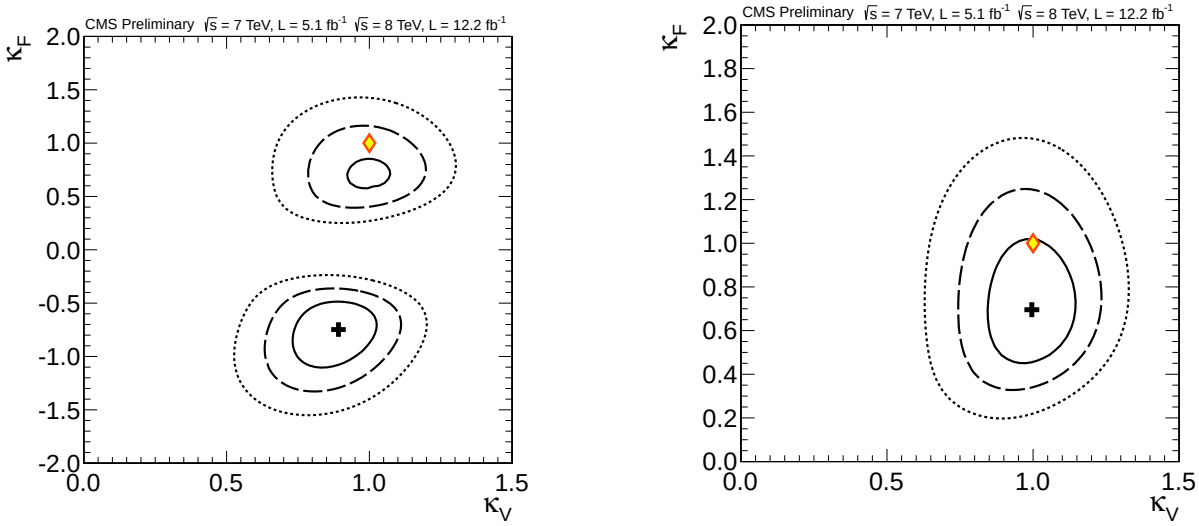

Figure 13: The 2D likelihood of the κ_{V} and κ_f parameters. The cross indicates the best-fit values. The solid, dashed and dotted contours show the 68%, 95% and 99.7% CL ranges, respectively. The yellow diamond shows the SM point $(\kappa_{\mathrm{V}}, \kappa_f) = (1, 1)$. The left plot shows the likelihood scan in two quadrants, (+,+) and (+,−). The right plot shows the likelihood scan constrained to the (+,+) quadrant.

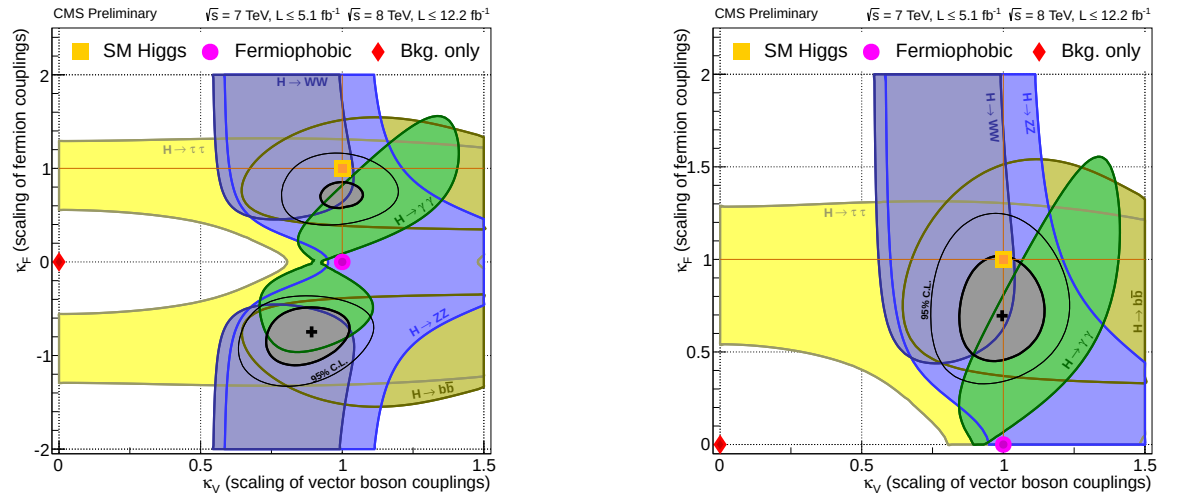

Figure 14: The 68% CL contours for individual channels (coloured swaths) and for the overall combination (solid line) for the $(\kappa_{\mathrm{V}}, \kappa_f)$ parameters. The cross indicates the global best-fit values. The thin contour shows the 95% CL range for the combination. The yellow diamond shows the SM point $(\kappa_{\mathrm{V}}, \kappa_f) = (1, 1)$. The left plot is the likelihood scan in two quadrants (+,+) and (+,−), the right plot—in the positive quadrant only.

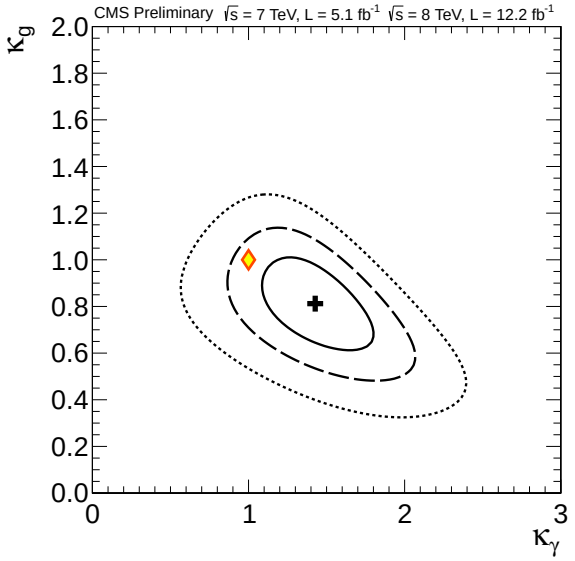

Figure 15: The 2D likelihood scan for κ_g and κ_γ parameters, assuming that $\Gamma_{\text{BSM}} = 0$, i.e. no new Higgs boson decay modes are open. The cross indicates the best-fit values. The solid, dashed and dotted contours show the 68%, 95% and 99.7% CL ranges, respectively. The yellow diamond shows the SM point $(\kappa_\gamma, \kappa_g) = (1, 1)$. The partial widths associated with the tree-level production processes and decay modes are assumed to be unaltered ($\kappa = 1$).

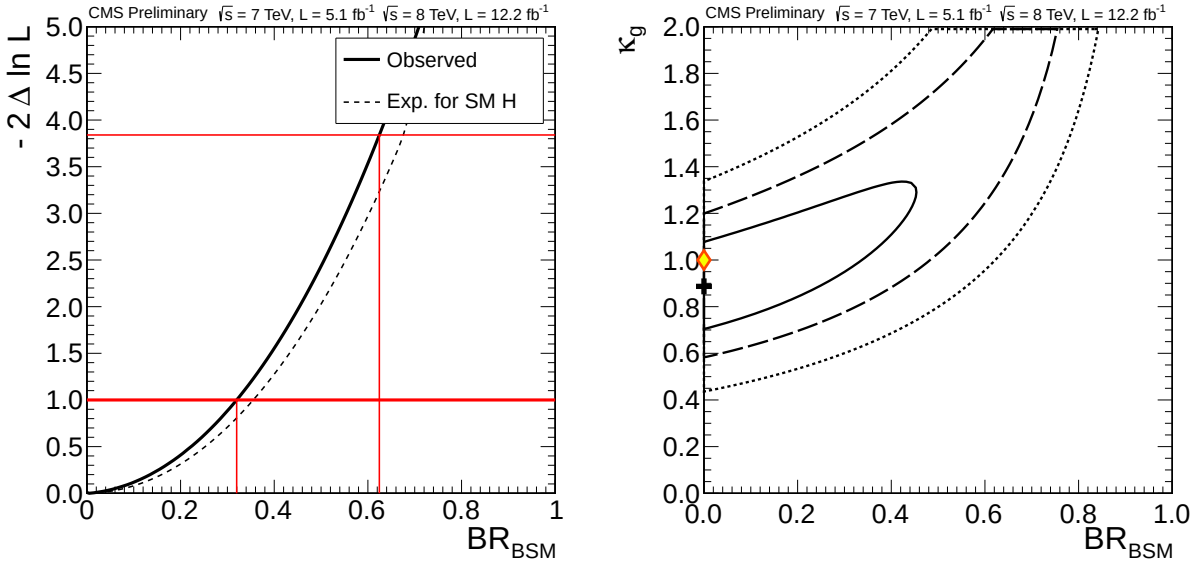

Figure 16: (Left) The likelihood scan versus $\text{BR}_{\text{BSM}} = \Gamma_{\text{BSM}}/\Gamma_{\text{tot}}$. The solid curve is the data and the dashed line indicates the expected median results in the presence of the SM Higgs boson. The partial widths associated with the tree-level production processes and decay modes are assumed to be unaltered ($\kappa = 1$). (Right) Correlation between κ_g and BR_{BSM}. The solid, dashed and dotted contours show the 68%, 95% and 99.7% CL ranges, respectively.

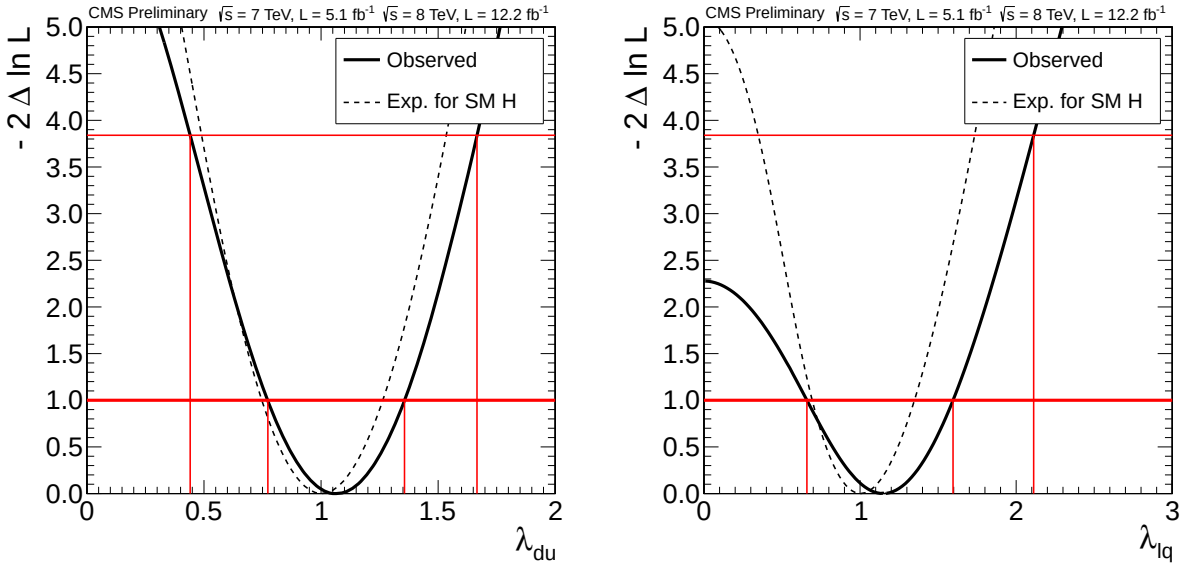

Figure 17: (Left) Likelihood scan vs ratio of couplings to down/up fermions λ_{du}, with the two other free coupling modifiers, κ_{v} and κ_{u}, profiled together with all other nuisance parameters. (Right) Likelihood scan vs ratio of couplings to leptons and quarks $\lambda_{\ell\mathrm{q}}$, with the two other free coupling modifiers, κ_{v} and κ_{q}, profiled together with all other nuisance parameters.

Test of the C6 model with six independent couplings

The C6 model makes the following assumptions:

- The couplings to W and Z bosons are scaled by a common factor κ_{V};
- The couplings to the 3rd generation fermions, top quark, bottom quark, and tau lepton, are scaled independently by κ_t, κ_b, κ_τ;
- The scale factors for couplings to the 1st and 2nd generation fermions are equal to those for the 3rd;
- The effective couplings to gluons and photons, induced by loop diagrams, are given independent scaling factors κ_g and κ_γ, respectively;
- The partial width Γ_{BSM} is zero.

This leaves the model with six independent parameters. The results of the fit for these six parameters, one at a time while profiling the remaining five together with all other nuisance parameters, are shown in Fig. 18. The current data do not show any statistically significant anomalies with respect to the SM Higgs boson hypothesis. For each κ, the measured 95% CL interval contains unity. A goodness-of-fit test between the parameters measured in this model and the SM prediction yields $\chi^2/\mathrm{n.d.f.} = 4.7/5$, which corresponds to an asymptotic p-value=0.58. The p-value obtained by generating a large number of pseudo-experiments is 0.57.

Summary of tests of the compatibility of the data with the SM Higgs boson couplings

Table 4 summarizes the tests performed on the compatibility of the data with the expected SM Higgs boson couplings. No statistically significant anomalies are observed.

4.5 Tests of different spin-parity hypotheses

The decay of the new boson to two photons implies that its spin is different from one [96, 97]. In this section we summarize results of testing the $\mathrm{J^P}$ hypotheses: 0^- vs. 0^+.

The only channel used in these tests is $\mathrm{X} \to \mathrm{ZZ} \to 4\ell$. The kinematic correlations between the four leptons in this decay mode are sensitive to the $\mathrm{J^P}$ properties of the decaying resonance. The state $\mathrm{J^P} = 0^+$ is assumed to be a scalar with a coupling structure to gluons and Z bosons equal to that of the SM Higgs boson. The exact definitions of the coupling structure of the pseudo-scalar state $\mathrm{J^P} = 0^-$ can be found in Ref. [79].

Figure 19 shows the expected distributions of test statistic $q = -2\ln(\mathcal{L}_{0^-\mathrm{+bkg}}/\mathcal{L}_{0^+\mathrm{+bkg}})$ for background and signal of two types, 0^- and 0^+ (SM Higgs boson), for $m_{\mathrm{H}} = 126$ GeV. The two likelihoods for the alternative hypotheses are maximized independently with respect to the nuisance parameters and the signal strength. The expected distributions are generated with a signal cross-section equal to that of the SM, which is consistent with the observation. We find that results do not change significantly if the expected distributions are generated with the measured signal strength. The observed value of test statistic q deviates from the median expected for the $J^P = 0^-$ hypothesis by 2.45 standard deviations and is consistent with the median expected for the $J^P = 0^+$ hypothesis within 0.53 standard deviations. The median for the SM 0^+ distribution lies 1.93 standard deviations into the tail of the 0^- distribution, while the median for the 0^- distribution lies 1.99 standard deviations into the tail of the 0^+ distribution. We define a $\mathrm{CL_s}$ criterion as the ratio of the probabilities to observe, under the 0^+ and 0^- hypotheses, values of the test statistics, q, equal or larger than the ones observed in the data. Under the assumption that the observed boson has spin zero, the data disfavour the

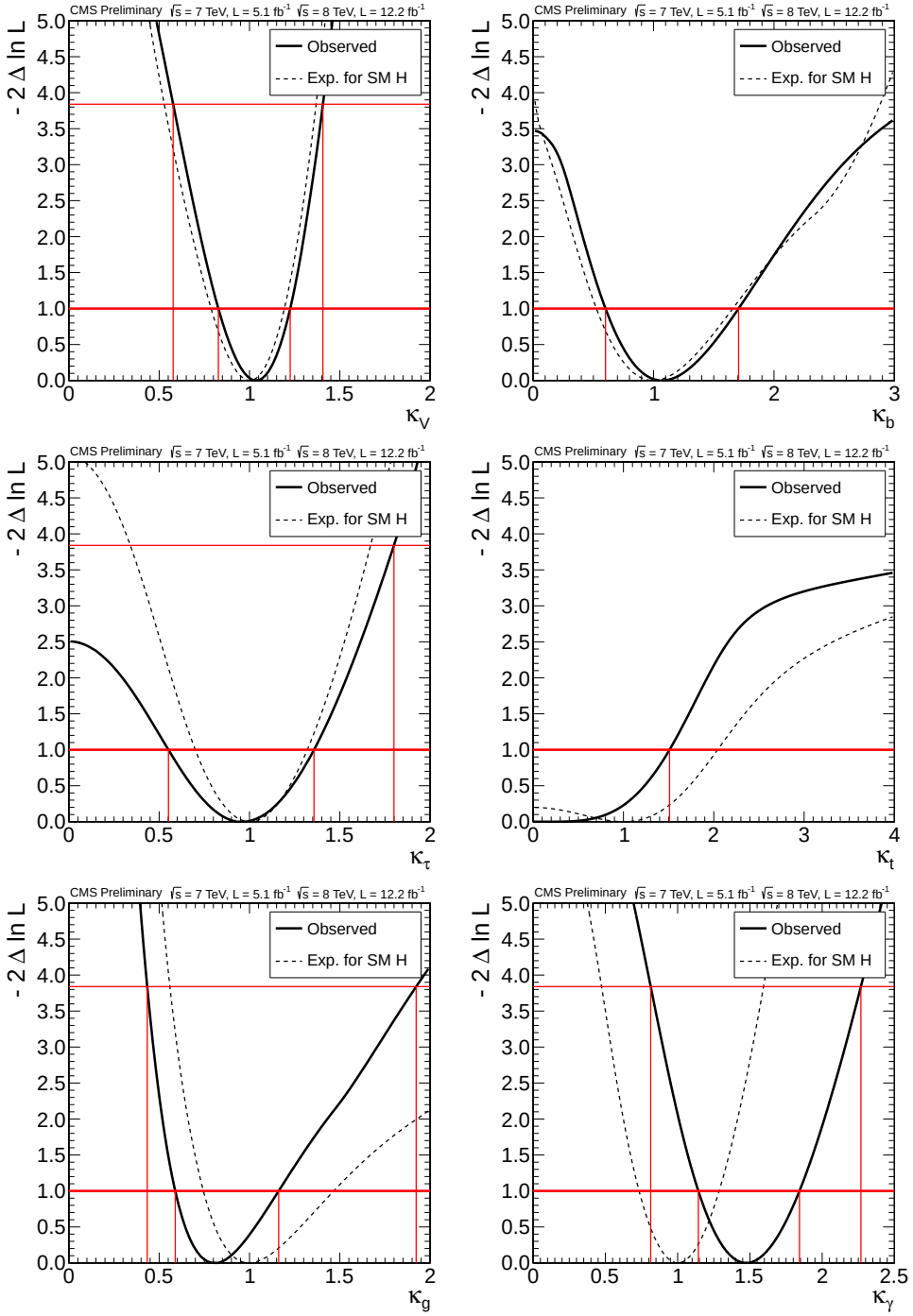

Figure 18: Data fit for six coupling scaling factors in the C6 model, one coupling at a time while profiling the remaining five together with all other nuisance parameters: (a) κ_V; (b) κ_b. (c) κ_τ. (d) κ_t. (e) κ_g. (f) κ_γ.

Table 4: Tests of the compatibility of the data with the SM Higgs boson couplings and the 95% CL intervals for evaluated scaling factors κ's. The different compatibility tests discussed in the text are separated by horizontal lines. When one of the scaling factors in a group is evaluated, others are treated as nuisance parameters. Scaling factors not listed explicitly in a group are taken to be unity.

Model parameters	Assessed scaling factors (95% CL intervals)		Comments
λ_{wz}, κ_{z}	λ_{wz}	[0.57,1.65]	Ratio of couplings to W and Z; ZZ and WW(0/1jet) channels only
λ_{wz}, κ_{z}, κ_f	λ_{wz}	[0.67,1.55]	Ratio of couplings to W and Z
κ_{v}	κ_{v}	[0.78,1.19]	Couplings to W/Z-bosons (V); $\kappa_f = 1$
κ_f	κ_f	[0.40,1.12]	Couplings to fermions (f); $\kappa_{\mathrm{v}} = 1$
κ_γ, κ_g	κ_γ	[0.98,1.92]	Couplings to photons (γ) and gluons (g)
	κ_g	[0.55,1.07]	(loop-induced couplings)
$\mathcal{B}(\mathrm{H} \to \mathrm{BSM})$, κ_γ, κ_g	$\mathcal{B}(\mathrm{H} \to \mathrm{BSM})$	[0.00,0.62]	Branching ratio for decays to BSM particles
λ_{du}, κ_{v}, κ_{u}	λ_{du}	[0.45,1.66]	Ratio of couplings to down and up-type fermions
$\lambda_{\ell\mathrm{q}}$, κ_{v}, κ_{q}	$\lambda_{\ell\mathrm{q}}$	[0.00,2.11]	Ratio of couplings to leptons and quarks
κ_{v}, κ_b, κ_τ, κ_t, κ_g, κ_γ	κ_{v}	[0.58,1.41]	Couplings to W/Z-bosons (V)
	κ_b	not constrained	Couplings to down-type quarks (b)
	κ_τ	[0.00,1.80]	Couplings to charged leptons (τ)
	κ_t	not constrained	Couplings to top-type quarks (t)
	κ_g	[0.43,1.92]	Effective couplings to gluons (g)
	κ_γ	[0.81,2.27]	Effective couplings to photons (γ)

pseudo-scalar hypothesis 0^- with a CL_s value of 2.4%.

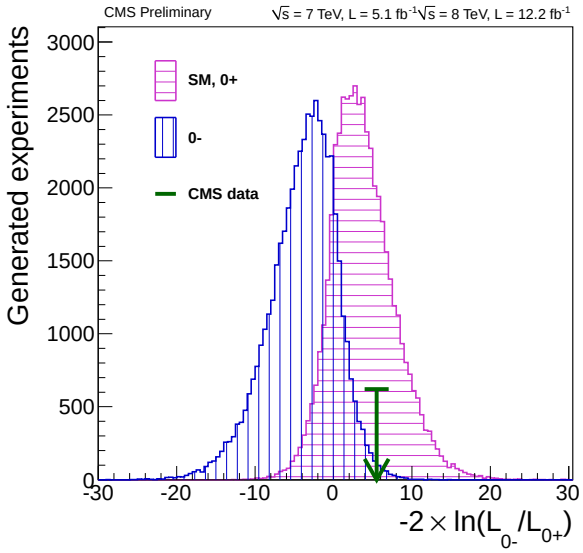

Figure 19: Expected distributions of the test statistic comparing the signal J^P hypotheses: 0^- vs 0^+. The observed value is indicated by the arrow.

5 Conclusions

Results are presented from searches for the standard model (SM) Higgs boson in proton-proton collisions at $\sqrt{s}$ = 7 and 8 TeV, using data samples corresponding to integrated luminosities of up to 5.1 fb^{-1} at 7 TeV and up to 12.2 fb^{-1} at 8 TeV. The search is performed in the mass range 110–1000 GeV in five decay modes: $\gamma\gamma$, ZZ, WW, $\tau\tau$, and bb. Updated results are presented except for the $\gamma\gamma$ mode. The significance of the recently discovered boson is now 6.9 σ. Its mass is measured to be 125.8 $\pm$ 0.4 (stat) $\pm$ 0.4 (syst) GeV. The event yields obtained by the different analyses targeting specific decay modes and production mechanisms are consistent with those expected for the SM Higgs boson. The best-fit signal strength for all channels combined, expressed in units of the SM Higgs boson cross section, is 0.88$\pm$0.21 at the measured mass. The consistency of the couplings of the observed boson with those predicted for the SM Higgs boson is tested in various ways, and no significant deviations are found. Under the assumption that the observed boson has spin zero, the data disfavour the pseudo-scalar hypothesis 0^- with a CL_s value of 2.4%.

References

[1] S. L. Glashow, "Partial-symmetries of weak interactions", *Nucl. Phys.* **22** (1961) 579, doi:10.1016/0029-5582(61)90469-2.

[2] S. Weinberg, "A Model of Leptons", *Phys. Rev. Lett.* **19** (1967) 1264, doi:10.1103/PhysRevLett.19.1264.

[3] A. Salam, "Weak and electromagnetic interactions", in *Elementary particle physics: relativistic groups and analyticity*, N. Svartholm, ed., p. 367. Almqvist & Wiskell, 1968. Proceedings of the eighth Nobel symposium.

[4] F. Englert and R. Brout, "Broken symmetry and the mass of gauge vector mesons", *Phys. Rev. Lett.* **13** (1964) 321, doi:10.1103/PhysRevLett.13.321.

[5] P. W. Higgs, "Broken symmetries, massless particles and gauge fields", *Phys. Lett.* **12** (1964) 132, doi:10.1016/0031-9163(64)91136-9.

[6] P. W. Higgs, "Broken symmetries and the masses of gauge bosons", *Phys. Rev. Lett.* **13** (1964) 508, doi:10.1103/PhysRevLett.13.508.

[7] G. S. Guralnik, C. R. Hagen, and T. W. B. Kibble, "Global conservation laws and massless particles", *Phys. Rev. Lett.* **13** (1964) 585, doi:10.1103/PhysRevLett.13.585.

[8] P. W. Higgs, "Spontaneous symmetry breakdown without massless bosons", *Phys. Rev.* **145** (1966) 1156, doi:10.1103/PhysRev.145.1156.

[9] T. W. B. Kibble, "Symmetry breaking in non-Abelian gauge theories", *Phys. Rev.* **155** (1967) 1554, doi:10.1103/PhysRev.155.1554.

[10] CMS Collaboration, "The CMS experiment at the CERN LHC", *JINST* **03** (2008) S08004, doi:10.1088/1748-0221/3/08/S08004.

[11] CMS Collaboration Collaboration, "Observation of a new boson at a mass of 125 GeV with the CMS experiment at the LHC", *Phys.Lett.* **B716** (2012) 30–61, doi:10.1016/j.physletb.2012.08.021, arXiv:1207.7235.

[12] ATLAS Collaboration Collaboration, "Observation of a new particle in the search for the Standard Model Higgs boson with the ATLAS detector at the LHC", *Phys.Lett.* **B716** (2012) 1–29, doi:10.1016/j.physletb.2012.08.020, arXiv:1207.7214.

[13] CMS Collaboration, "The CMS experiment at the CERN LHC", *JINST* **3** (2008) S08004, doi:10.1088/1748-0221/3/08/S08004.

[14] J. R. Ellis, M. K. Gaillard, and D. V. Nanopoulos, "A phenomenological profile of the Higgs boson", *Nucl. Phys. B* **106** (1976) 292, doi:10.1016/0550-3213(76)90382-5.

[15] H. M. Georgi, S. L. Glashow, M. E. Machacek et al., "Higgs Bosons from Two Gluon Annihilation in Proton Proton Collisions", *Phys. Rev. Lett.* **40** (1978) 692, doi:10.1103/PhysRevLett.40.692.

[16] S. L. Glashow, D. V. Nanopoulos, and A. Yildiz, "Associated Production of Higgs Bosons and Z Particles", *Phys. Rev. D* **18** (1978) 1724, doi:10.1103/PhysRevD.18.1724.

[17] R. N. Cahn, S. D. Ellis, R. Kleiss et al., "Transverse Momentum Signatures for Heavy Higgs Bosons", *Phys. Rev. D* **35** (1987) 1626, doi:10.1103/PhysRevD.35.1626.

[18] D. L. Rainwater and D. Zeppenfeld, "Searching for H $\to \gamma\gamma$ in weak boson fusion at the LHC", *JHEP* **12** (1997) 005, doi:10.1088/1126-6708/1997/12/005, arXiv:hep-ph/9712271.

[19] D. L. Rainwater, D. Zeppenfeld, and K. Hagiwara, "Searching for H $\to \tau\tau$ in weak boson fusion at the CERN LHC", *Phys. Rev. D* **59** (1998) 014037, doi:10.1103/PhysRevD.59.014037, arXiv:hep-ph/9808468.

[20] D. L. Rainwater and D. Zeppenfeld, "Observing $H \to W^{(*)}W^{(*)} \to e^{\pm}\mu^{\mp} \not{p}_T$ in weak boson fusion with dual forward jet tagging at the CERN LHC", *Phys. Rev. D* **60** (1999) 113004, doi:10.1103/PhysRevD.60.113004, arXiv:hep-ph/9906218. Also Erratum, Doi=10.1103/PhysRevD.61.099901.

[21] LHC Higgs Cross Section Working Group, S. Dittmaier, C. Mariotti et al., "Handbook of LHC Higgs Cross Sections: 1. Inclusive Observables", (CERN, Geneva, 2011). arXiv:1101.0593.

[22] LHC Higgs Cross Section Working Group, S. Dittmaier, C. Mariotti et al., "Handbook of LHC Higgs Cross Sections: 2. Differential Distributions", (CERN, Geneva, 2012). arXiv:1201.3084.

[23] LHC Higgs Cross Section Working Group, "Higgs Cross Sections at 7 and 8 TeV", (2012).

[24] A. Djouadi, M. Spira, and P. M. Zerwas, "Production of Higgs bosons in proton colliders: QCD corrections", *Phys. Lett. B* **264** (1991) 440, doi:10.1016/0370-2693(91)90375-Z.

[25] S. Dawson, "Radiative corrections to Higgs boson production", *Nucl. Phys. B* **359** (1991) 283, doi:10.1016/0550-3213(91)90061-2.

[26] M. Spira, A. Djouadi, D. Graudenz et al., "Higgs boson production at the LHC", *Nucl. Phys. B* **453** (1995) 17, doi:10.1016/0550-3213(95)00379-7, arXiv:hep-ph/9504378.

[27] R. V. Harlander and W. B. Kilgore, "Next-to-next-to-leading order Higgs production at hadron colliders", *Phys. Rev. Lett.* **88** (2002) 201801, doi:10.1103/PhysRevLett.88.201801, arXiv:hep-ph/0201206.

[28] C. Anastasiou and K. Melnikov, "Higgs boson production at hadron colliders in NNLO QCD", *Nucl. Phys. B* **646** (2002) 220, doi:10.1016/S0550-3213(02)00837-4, arXiv:hep-ph/0207004.

[29] V. Ravindran, J. Smith, and W. L. van Neerven, "NNLO corrections to the total cross section for Higgs boson production in hadron hadron collisions", *Nucl. Phys. B* **665** (2003) 325, doi:10.1016/S0550-3213(03)00457-7, arXiv:hep-ph/0302135.

[30] S. Catani, D. de Florian, M. Grazzini et al., "Soft-gluon resummation for Higgs boson production at hadron colliders", *JHEP* **07** (2003) 028, doi:10.1088/1126-6708/2003/07/028.

[31] U. Aglietti, R. Bonciani, G. Degrassi et al., "Two-loop light fermion contribution to Higgs production and decays", *Phys. Lett. B* **595** (2004) 432, doi:10.1016/j.physletb.2004.06.063, arXiv:hep-ph/0404071.

[32] G. Degrassi and F. Maltoni, "Two-loop electroweak corrections to Higgs production at hadron colliders", *Phys. Lett. B* **600** (2004) 255, doi:10.1016/j.physletb.2004.09.008, arXiv:hep-ph/0407249.

[33] S. Actis, G. Passarino, C. Sturm et al., "NLO Electroweak Corrections to Higgs Boson Production at Hadron Colliders", *Phys. Lett. B* **670** (2008) 12, doi:10.1016/j.physletb.2008.10.018, arXiv:0809.1301.

[34] C. Anastasiou, R. Boughezal, and F. Petriello, "Mixed QCD-electroweak corrections to Higgs boson production in gluon fusion", *JHEP* **04** (2009) 003, doi:10.1088/1126-6708/2009/04/003, arXiv:0811.3458.

[35] D. de Florian and M. Grazzini, "Higgs production through gluon fusion: updated cross sections at the Tevatron and the LHC", *Phys. Lett. B* **674** (2009) 291, doi:10.1016/j.physletb.2009.03.033, arXiv:0901.2427.

[36] J. Baglio and A. Djouadi, "Higgs production at the lHC", *JHEP* **03** (2011) 055, doi:10.1007/JHEP03(2011)055, arXiv:1012.0530.

[37] D. de Florian and M. Grazzini, "Higgs production at the LHC: updated cross sections at $\sqrt{s} = 8$ TeV", (2012). arXiv:1206.4133.

[38] C. Anastasiou, S. Buehler, F. Herzog et al., "Inclusive Higgs boson cross-section for the LHC at 8 TeV", *JHEP* **04** (2012) 004, doi:10.1007/JHEP04(2012)004, arXiv:1202.3638.

[39] G. Bozzi, S. Catani, D. de Florian et al., "Transverse-momentum resummation and the spectrum of the Higgs boson at the LHC", *Nucl. Phys. B* **737** (2006) 73, doi:10.1016/j.nuclphysb.2005.12.022, arXiv:hep-ph/0508068.

[40] D. de Florian, G. Ferrera, M. Grazzini et al., "Transverse-momentum resummation: Higgs boson production at the Tevatron and the LHC", *JHEP* **11** (2011) 064, doi:10.1007/JHEP11(2011)064.

[41] G. Passarino, C. Sturm, and S. Uccirati, "Higgs Pseudo-Observables, Second Riemann Sheet and All That", *Nucl. Phys. B* **834** (2010) 77, doi:10.1016/j.nuclphysb.2010.03.013, arXiv:1001.3360.

[42] I. W. Stewart and F. J. Tackmann, "Theory Uncertainties for Higgs and Other Searches Using Jet Bins", *Phys. Rev. D* **85** (2012) 034011, doi:10.1103/PhysRevD.85.034011, arXiv:1107.2117.

[43] A. Djouadi, J. Kalinowski, and M. Spira, "HDECAY: A program for Higgs boson decays in the standard model and its supersymmetric extension", *Comput. Phys. Commun.* **108** (1998) 56, doi:10.1016/S0010-4655(97)00123-9, arXiv:hep-ph/9704448.

[44] A. Djouadi, J. Kalinowski, M. Muhlleitner et al., "An update of the program HDECAY", in *The Les Houches 2009 workshop on TeV colliders: The tools and Monte Carlo working group summary report*. 2010. arXiv:1003.1643.

[45] A. Bredenstein, A. Denner, S. Dittmaier et al., "Precise predictions for the Higgs-boson decay H $\to$ WW/ZZ $\to$ 4 leptons", *Phys. Rev. D* **74** (2006) 013004, doi:10.1103/PhysRevD.74.013004, arXiv:hep-ph/0604011.

[46] A. Bredenstein, A. Denner, S. Dittmaier et al., "Radiative corrections to the semileptonic and hadronic Higgs-boson decays H $\to$WW/ZZ$\to$ 4 fermions", *JHEP* **02** (2007) 080, doi:10.1088/1126-6708/2007/02/080, arXiv:hep-ph/0611234.

[47] S. Actis, G. Passarino, C. Sturm et al., "NNLO Computational Techniques: the Cases $H \to \gamma\gamma$ and $H \to gg$", *Nucl. Phys. B* **811** (2009) 182, doi:10.1016/j.nuclphysb.2008.11.024, arXiv:0809.3667.

[48] A. Denner, S. Heinemeyer, I. Puljak et al., "Standard Model Higgs-Boson Branching Ratios with Uncertainties", *Eur. Phys. J. C* **71** (2011) 1753, doi:10.1140/epjc/s10052-011-1753-8, arXiv:1107.5909.

[49] M. Ciccolini, A. Denner, and S. Dittmaier, "Strong and Electroweak Corrections to the Production of a Higgs Boson+2 Jets via Weak Interactions at the Large Hadron Collider", *Phys. Rev. Lett.* **99** (2007) 161803, doi:10.1103/PhysRevLett.99.161803, arXiv:0707.0381.

[50] M. Ciccolini, A. Denner, and S. Dittmaier, "Electroweak and QCD corrections to Higgs production via vector-boson fusion at the LHC", *Phys. Rev. D* **77** (2008) 013002, doi:10.1103/PhysRevD.77.013002, arXiv:0710.4749.

[51] T. Figy, C. Oleari, and D. Zeppenfeld, "Next-to-leading order jet distributions for Higgs boson production via weak-boson fusion", *Phys. Rev. D* **68** (2003) 073005, doi:10.1103/PhysRevD.68.073005, arXiv:hep-ph/0306109.

[52] K. Arnold, M. Bahr, G. Bozzi et al., "VBFNLO: A parton level Monte Carlo for processes with electroweak bosons", *Comput. Phys. Commun.* **180** (2009) 1661, doi:10.1016/j.cpc.2009.03.006, arXiv:0811.4559.

[53] P. Bolzoni, F. Maltoni, S.-O. Moch et al., "Higgs production via vector-boson fusion at NNLO in QCD", *Phys. Rev. Lett.* **105** (2010) 011801, doi:10.1103/PhysRevLett.105.011801, arXiv:1003.4451.

[54] T. Han and S. Willenbrock, "QCD correction to the $pp \to WH$ and ZH total cross-sections", *Phys. Lett. B* **273** (1991) 167, doi:10.1016/0370-2693(91)90572-8.

[55] O. Brein, A. Djouadi, and R. Harlander, "NNLO QCD corrections to the Higgs-strahlung processes at hadron colliders", *Phys. Lett. B* **579** (2004) 149, doi:10.1016/j.physletb.2003.10.112, arXiv:hep-ph/0307206.

[56] M. L. Ciccolini, S. Dittmaier, and M. Krämer, "Electroweak radiative corrections to associated WH and ZH production at hadron colliders", *Phys. Rev. D* **68** (2003) 073003, doi:10.1103/PhysRevD.68.073003, arXiv:hep-ph/0306234.

[57] R. Hamberg, W. L. van Neerven, and T. Matsuura, "A complete calculation of the order α_S^2 correction to the Drell-Yan K factor", *Nucl. Phys. B* **359** (1991) 343, doi:10.1016/0550-3213(91)90064-5.

[58] A. Denner, S. Dittmaier, S. Kallweit et al., "EW corrections to Higgs strahlung at the Tevatron and the LHC with HAWK", (2011). arXiv:1112.5258.

[59] G. Ferrera, M. Grazzini, and F. Tramontano, "Associated WH production at hadron colliders: a fully exclusive QCD calculation at NNLO", *Phys. Rev. Lett.* **107** (2011) 152003, doi:10.1103/PhysRevLett.107.152003, arXiv:1107.1164.

[60] W. Beenakker, S. Dittmaier, M. Kramer et al., "Higgs radiation off top quarks at the Tevatron and the LHC", *Phys. Rev. Lett.* **87** (2001) 201805, doi:10.1103/PhysRevLett.87.201805, arXiv:hep-ph/0107081.

[61] W. Beenakker, S. Dittmaier, M. Kramer et al., "NLO QCD corrections to $t\bar{t}$ H production in hadron collisions.", *Nucl. Phys. B* **653** (2003) 151, doi:10.1016/S0550-3213(03)00044-0, arXiv:hep-ph/0211352.

[62] S. Dawson, L. H. Orr, L. Reina et al., "Associated top quark Higgs boson production at the LHC", *Phys. Rev. D* **67** (2003) 071503, doi:10.1103/PhysRevD.67.071503, arXiv:hep-ph/0211438.

[63] S. Dawson, C. Jackson, L. H. Orr et al., "Associated Higgs production with top quarks at the Large Hadron Collider: NLO QCD corrections", *Phys. Rev. D* **68** (2003) 034022, doi:10.1103/PhysRevD.68.034022, arXiv:hep-ph/0305087.

[64] M. Botje et al., "The PDF4LHC Working Group Interim Recommendations", arXiv:1101.0538.

[65] S. Alekhin et al., "The PDF4LHC Working Group Interim Report", arXiv:1101.0536.

[66] H. Lai et al., "New parton distributions for collider physics", *Phys. Rev. D* **82** (2010) 074024, doi:10.1103/PhysRevD.82.074024, arXiv:1007.2241.

[67] A. Martin et al., "Parton distributions for the LHC", *Eur.Phys.J. C* **63** (2009) 189, doi:10.1140/epjc/s10052-009-1072-5, arXiv:0901.0002.

[68] NNPDF Collaboration, "Impact of Heavy Quark Masses on Parton Distributions and LHC Phenomenology", *Nucl. Phys. B* **849** (2011) 296, doi:10.1016/j.nuclphysb.2011.03.021, arXiv:1101.1300.

[69] CMS Collaboration, "Search for a standard model Higgs boson decaying into two photons in pp collisions", *CMS Physics Analysis Summary* **CMS-PAS-HIG-12-015** (2012).

[70] CMS Collaboration, "Search for standard model Higgs bosons produced in association with W or Z bosons, and decayng to bottom quarks", *CMS Physics Analysis Summary* **CMS-PAS-HIG-12-044** (2012).

[71] CMS Collaboration, "Search for Higgs production in association with top quark pairs in pp collisions", *CMS Physics Analysis Summary* **CMS-PAS-HIG-12-025** (2012).

[72] CMS Collaboration, "Search for standard model Higgs bosons decaying to tau pairs", *CMS Physics Analysis Summary* **CMS-PAS-HIG-12-043** (2012).

[73] CMS Collaboration, "Search for a Standard Model Higgs bosons decaying to tau pairs produced in association with a W or a Z boson", *CMS Physics Analysis Summary* **CMS-PAS-HIG-12-051** (2012).

[74] CMS Collaboration, "Search for the Standard Model Higgs boson in the $H \to WW \to lvjj$ decay channel", *CMS Physics Analysis Summary* **CMS-PAS-HIG-12-003** (2012).

[75] CMS Collaboration, "Search for a Standard Model Higgs boson in the $H \to WW \to lvjj$ decay channel in pp collisions at $\sqrt{s}$s = 8 TeV", *CMS Physics Analysis Summary* **CMS-PAS-HIG-12-046** (2012).

[76] CMS Collaboration, "Search for the Higgs Boson Decaying to W^+W^- in the Fully Leptonic Final State", *CMS Physics Analysis Summary* **CMS-PAS-HIG-11-024** (2011).

[77] CMS Collaboration, "Evidence for a particle decaying into W^+W^- in the fully leptonic final state in a standard model Higgs bosons search in pp collisions at $\sqrt{s}$ = 8 TeV", *CMS Physics Analysis Summary* **CMS-PAS-HIG-12-042** (2012).

[78] CMS Collaboration, "Study of associated Higgs boson (WH) Production in the three leptons final state at 7 TeV", *CMS Physics Analysis Summary* **CMS-PAS-HIG-11-034** (2011).

[79] CMS Collaboration, "Discovery of a new boson in the search for the standard model Higgs bosons in the $H \to ZZ \to 4\ell$ channel in pp collisions at $\sqrt{s}$ = 7 and 8 TeV", *CMS Physics Analysis Summary* **CMS-PAS-HIG-12-041** (2012).

[80] CMS Collaboration, "Search for the standard model Higgs boson in the $H \to ZZ \to 4l$ channel in pp collisions at $\sqrt{s}$ = 7 and 8 TeV", *CMS Physics Analysis Summary* **CMS-PAS-HIG-12-016** (2012).

[81] S. Goria, G. Passarino, and D. Rosco, "The Higgs Boson Lineshape", *Nucl.Phys.* **B864** (2012) 530–579, doi:10.1016/j.nuclphysb.2012.07.006, arXiv:1112.5517.

[82] N. Kauer and G. Passarino, "Inadequacy of zero-width approximation for a light Higgs boson signal", *JHEP* **1208** (2012) 116, doi:10.1007/JHEP08(2012)116, arXiv:1206.4803.

[83] G. Passarino, "Higgs Interference Effects in $gg \to ZZ$ and their Uncertainty", *JHEP* **1208** (2012) 146, doi:10.1007/JHEP08(2012)146, arXiv:1206.3824.

[84] N. Kauer, "Signal-background interference in $gg \to H \to VV$", arXiv:1201.1667.

[85] Hirschi, Frixione, Laureys, Maltoni, "Higgs boson production through gluon fusion in MC@NLO", arXiv:to be published.

[86] R. E. J. M. Campbell and C. Williams., "Gluon-Gluon Contributions to W+ W- Production and Higgs Interference Effects", *JHEP* **1110** (2011) 0055, doi:10.1007/JHEP10(2011)005, arXiv:1107.5569.

[87] ATLAS and CMS Collaborations, LHC Higgs Combination Group, "Procedure for the LHC Higgs boson search combination in Summer 2011", Technical Report ATL-PHYS-PUB 2011-11, CMS NOTE 2011/005, (2011).

[88] CMS Collaboration, "Combined results of searches for the standard model Higgs boson in pp collisions at $\sqrt{s} = 7$ TeV", *Phys. Lett. B* **710** (2012) 26, doi:10.1016/j.physletb.2012.02.064, arXiv:1202.1488.

[89] G. Cowan, K. Cranmer, E. Gross et al., "Asymptotic formulae for likelihood-based tests of new physics", *Eur. Phys. J. C* **71** (2011) 1, doi:10.1140/epjc/s10052-011-1554-0, arXiv:1007.1727.

[90] L. Moneta, K. Belasco, K. S. Cranmer et al., "The RooStats Project", in *13th International Workshop on Advanced Computing and Analysis Techniques in Physics Research (ACAT2010)*. SISSA, 2010. arXiv:1009.1003. PoS(ACAT2010)057.

[91] T. Junk, "Confidence level computation for combining searches with small statistics", *Nucl. Instrum. Meth. A* **434** (1999) 435, doi:10.1016/S0168-9002(99)00498-2.

[92] A. L. Read, "Presentation of search results: the CLs technique", *J. Phys. G* **28** (2002) 2693, doi:10.1088/0954-3899/28/10/313.

[93] CMS Collaboration, "Observation of a resonance with a mass near 125 GeV in the search for the Higgs boson in pp collisions at $\sqrt{s} = 7$ and 8 TeV", *CMS Physics Analysis Summary* **CMS-PAS-HIG-12-020** (2012).

[94] LHC Higgs Cross Section Working Group, and David, A. and Denner, A. and Duehrssen, M. and Grazzini, M. and others, "LHC HXSWG interim recommendations to explore the coupling structure of a Higgs-like particle", arXiv:1209.0040.

[95] P. Sikivie, L. Susskind, M. B. Voloshin et al., "Isospin Breaking in Technicolor Models", *Nucl.Phys.* **B173** (1980) 189, doi:10.1016/0550-3213(80)90214-X.

[96] L. D. Landau, "On the angular momentum of a two-photon system", *Dokl. Akad. Nauk* **60** (1948) 207.

[97] C. N. Yang, "Selection Rules for the Dematerialization of a Particle into Two Photons", *Phys. Rev.* **77** (1950) 242, doi:10.1103/PhysRev.77.242.